13 Modeling Feature Selectivity in Local Cortical Circuits

David Hansel and Haim Sompolinsky

13.1 Introduction

Neuronal representations of the external world are often based on the selectivity of the responses of individual neurons to external features. For example, many neurons in visual cortex respond preferentially to visual stimuli that have a specific orientation (Hubel and Wiesel 1959), spatial frequency (Campbell et al. 1969), color (Hubel and Wiesel 1968), velocity and direction of motion (Orban 1984). In motor systems, neuronal activities are tuned to parameters of a planned action such as the direction of an arm reaching movement (Georgopoulos, Taira, and Lukashin 1993), or the direction of a saccadic eye movement (for a review, see Sparks and Mays 1990). It is often assumed that the primary mechanism underlying the response properties of a neuron resides in the transformations of sensory signals by feedforward filtering along afferent pathways (e.g., Hubel and Wiesel 1962). Although, in some cases, the feedforward model is consistent with our understanding of the nature of afferent inputs (Reid and Alonso 1995; Chapman, Zahs, and Stryker 1991), in others, particularly in motor areas, the relation between afferent inputs and cortical neuronal response properties is not obvious. Moreover, neurons in cortex, even in the input stages of primary sensory areas, receive most of their excitatory inputs from *cortical* sources rather than from afferent thalamic nuclei (Levay and Gilbert 1976; Peters and Payne 1993; Ahmed et al. 1994; Pei et al. 1994; Douglas et al. 1995). Cortical responses are also modulated by strong inputs from inhibitory cortical interneurons (Sillito 1977; Tsumoto, Eckart, and Creutzfeldt 1979; Sillito et al. 1980; Ferster and Koch 1987; Hata et al. 1988; Nelson et al. 1994). These facts and other experimental and theoretical considerations suggest that local cortical circuits may play an important role is shaping neuronal responses in cortex.

In this chapter we review the theoretical study of the function of local networks in cortex in relation to feature selectivity. By "local network" we mean an ensemble of neurons that respond to the same patch of the external world and are interconnected by recurrent synaptic connections. Typically, a local network spans roughly 1 mm^2 of cortical surface and is assumed to consist of subgroups of neurons each of which is tuned to a particular feature of an external stimulus. These subgroups will be called "feature columns" and the whole network a "hypercolumn," in analogy with the "ice cube" model of primary visual cortex (Hubel 1988; for a review of local cortical circuitry, see Martin 1988; Gilbert 1992; Abeles 1991).

The complexity of neuronal dynamics and circuitry in cortex precludes systematic investigation of the properties of realistic large-scale neuronal models of local cor-

tical circuits within a reasonable range of their parameter space (see chapter 12, this volume). Therefore simplified abstract models offer very valuable theoretical tools to gain insight into the working of these systems. Not only is the reduced parameter space of these simplified models significantly easier to search, but many are amenable to analytical investigations. Analytical solutions are extremely useful in that they often explicitly reveal the important relationships between a dynamic property of the network and some of its parameters. A primary goal of this chapter is to describe the application of analytical methods to simplified network models and their solutions. We will study models known as "neuronal rate models" or "neuronal population dynamics" (Wilson and Cowan 1972; Ginzburg and Sompolinsky 1994), in which the state of each neuron is characterized by a single continuous variable representing its activity level averaged over a short period of time. Similar models are the analog circuit equations for neural networks (Hopfield 1984). Although these models obviously cannot exhibit the complex dynamics of real neurons and circuits, they can account for some of the emergent cooperative properties that are either stationary or evolve on relatively slow time scales. To demonstrate the relevance of the simplified models to realistic situations, we will also describe in detail numerical simulations of networks consisting of conductance-based models of cortical neurons and synapses. (See also chapters 5 and 10, this volume.)

The present study focuses on networks that code the value of a single feature variable of the external stimulus, and thus have a one-dimensional functional architecture. The spectrum of possible spatiotemporal patterns of activity in such networks can be rich. We will restrict our attention to relatively simple spatial patterns consisting of a single domain of high activity, sometimes called an "activity hill." We will also consider the cases of 'moving hills' of activity, where the activity profile is not static but propagates across the network, successively activating neighboring columns. We will study the conditions for the emergence of these patterns and analyze which of their properties depend on the intrinsic circuit parameters and which, on the properties of the external stimulus.

Modeling of neuronal functions by static and moving *localized* spatial patterns in one-dimensional nonlinear neural networks dates back to Didday's model on the frog tectal bug detection system (Didday 1976) and the reticular formation model for behavioral mode selection of Kilmer, McCulloch and Blum (1969); (see Amari and Arbib 1977; and Montalvo 1975 for reviews of these and other models). Theoretical analysis of these patterns has been pioneered by Amari (1977). The difference between Amari's theory and the present work will be elucidated in section 13.8. *Global* spatiotemporal patterns in one- (and two-) dimensional networks have been studied also by Ermentrout and Cowan (see Ermentrout 1982 for review). More recently, localized

patterns in one- and two-dimensional neuronal rate models have been studied in relation to orientation selectivity in primary visual cortex (Ben-Yishai, Lev Bar-Or, and Sompolinsky 1995; Ben-Yishai, Hansel, and Sompolinsky 1997), the coding of direction of arm movements in motor cortex (Lukashin and Georgopoulos 1993; Lukashin et al. 1996), head direction tuning in the limbic systems (Redish, Elga, and Touretzky 1996; Zhang 1996), and the control of saccadic eye movements (Droulez and Berthoz 1991; Schierwagen and Werner 1996; Kopecz and Schöner 1995). The mechanisms underlying the emergence of spatiotemporal patterns of the types described above are quite universal. For this reason, here these models will be studied in the general context of coding of a one-dimensional feature (detailed applications to concrete cortical systems can be found in the recent literature devoted to these models).

The network models examined here are characterized by a strong internal recurrency, which gives rise to intrinsic stable static or dynamic patterns, called "attractors" (for a review of dynamical systems theory see, for example, Strogatz 1994). Computation by attractors has been studied in recent years in relation to associative memory and optimization problems (Hopfield 1982, 1984; Hopfield and Tank 1986; Amit, Gutfreund, and Sompolinsky 1985; Amit 1989). The models we will be examining differ in that their intrinsic stable states are not isolated points in configuration space (the space of all possible instantaneous states of the system) but form a continuous line in this space. Recently a network model with line attractor has been studied as a mechanism for gaze holding by Seung (1996) and by Lee et al. (1996). We will briefly compare these models in section 13.8.

Section 13.2 describes our network model's basic architecture and defines the network's rate dynamics of excitatory and inhibitory populations in a hypercolumn. Section 13.3 further simplifies the model by collapsing the excitatory and inhibitory populations into a single "equivalent" population; this one-population rate model serves as the basis of our subsequent analytical investigations. Section 13.4 explores the properties of static activity profiles that emerge in the case of a uniform external stimulus and in response to a spatially tuned stimulus. We will analyze in detail how cortical feedback shapes the emergent activity profile.

Section 13.5 examines, first, the network response to a "moving" external stimulus (one whose feature value changes with time), where an interesting issue is the network's ability to lock to the moving stimulus. Our investigation also illustrates the usefulness of phase dynamics (see chapter 7, this volume) in describing how a spatiotemporal pattern is phase- and frequency-locked to an external force. We next discuss the emergence of *intrinsic* moving profiles in networks with static uniform stimulus. Propagating pulses are known to exist in excitable one-dimensional media, such as the propagation of action potential along a nerve's axon (Hodgkin and

Huxley 1952; Rinzel and Keller 1973; Tuckwell 1988). Here we study a mechanism for generating moving localized activity profiles in neural networks which is based on neuronal adaptation. We incorporate neuronal adaptation current into the one-population rate model by a simple phenomenological model of a slow, local negative linear feedback, showing that, for sufficiently strong adaptation, the static hills become destabilized and that propagating hills of activity become the stable states of the system instead. We briefly discuss the interaction between the intrinsic moving hills and an external tuned static stimulus.

A central issue of this chapter is the relation between the spatial modulation of the external input, as well as the cortical interactions, and the emergent tuning of the network responses. In the model studied in sections 13.2–13.5, the spatial modulations of the internal and external inputs are characterized by their spatial modulation *depth*. Their range, however, is assumed to be long and fixed. An important question is the role of the spatial *width* of the synaptic interactions or of the external input on the emergent spatial activity profile. This is the topic of section 13.6, which presents a solution to a model where both the excitatory interactions and the external input are exponentially decreasing functions of distance. Although more complex, this model can still be solved analytically, and it enables us to elucidate the role of both the spatial modulation depth and the spatial range of the synaptic inputs.

Section 13.7 considers a network model that incorporates realistic conductance-based dynamics appropriate for cortical neurons, whose architecture is similar to the rate models, except that the network consists of separate excitatory and inhibitory populations. Many aspects of the simulations, including the size dependence of the network behavior and the classification of its synchrony and temporal variability, are described in detail in Hansel and Sompolinsky (1996). Here we focus mainly on results directly relevant to the comparison with the predictions of the rate model. We first show that under certain conditions the state of these networks can also be described by self-consistent rate equations. We then proceed to present the results of numerical simulations of this model, and compare them with the predictions of the rate model. The results are also briefly discussed in our conclusion, section 13.8.

13.2 Model of a Cortical Hypercolumn

13.2.1 Network Architecture

We consider a network of neurons that code for a sensory or movement feature. The feature is assumed to be a scalar denoted by θ, with a finite range of values (in most of this chapter, $-\pi/2 \leq \theta < \pi/2$). For simplicity, we will assume periodic boundary

conditions, so that θ can be considered an angle, and all functions of θ will be periodic functions with period π. In section 13.6 we will consider the more general case where θ is not an angle variable, so that the boundary conditions are not periodic.

Each neuron in the hypercolumn is selective to a particular range of feature values, and fires maximally when a feature with a particular value is present. This value is called the "preferred feature" (PF) of the neuron. The network consists of N_E excitatory neurons and N_I inhibitory neurons, parametrized by a coordinate θ, which denotes their PF. The PFs are assumed to be distributed uniformly between $-\pi/2$ and $+\pi/2$. An additional N_0 neuron provides external input to the network. These external sources are typically excitatory afferent currents induced by sensory stimulation. We will refer to this input as the "stimulus input" of the network. We denote an excitatory neuron by an index E and an inhibitory one by I. The external excitatory neurons are denoted by 0.

Each neuron receives a synaptic current, $I^{\alpha}(\theta, t)$, where $\alpha = E, I$ denotes the type of the neuron, θ its PF, and t denotes time. This current consists of three components:

$$I^{\alpha}(\theta, t) = I^{\alpha E}(\theta, t) + I^{\alpha I}(\theta, t) + I^{\alpha 0}(\theta, t), \tag{13.1}$$

where $I^{\alpha\beta}(\theta, t)$ is the synaptic current on a θ neuron in the αth population generated by the activity of the βth population, and $I^{\alpha 0}(\theta, t)$ stands for synaptic currents from the external neurons. The synaptic currents $I^{\alpha\beta}$ are each a sum of synaptic inputs from individual neurons mediated by pairwise synaptic interactions. The synaptic efficacy between a presynaptic *excitatory* neuron, θ', and a postsynaptic neuron, θ of type α, is denoted by $(1/N_E)J^{\alpha E}(|\theta - \theta'|)$. The interaction strength between a presynaptic *inhibitory* neuron, θ', and a postsynaptic neuron, θ of type α, is denoted by $(1/N_I)J^{\alpha I}(|\theta - \theta'|)$. The functions $J^{\alpha\beta}(\theta)$ represent the dependence of the interaction between neurons on the similarity of their PFs. Both excitatory and the inhibitory interactions are assumed to be strongest in magnitude for neurons that have identical PFs. This hypothesis is consistent with the anatomical and physiological evidence available in primary visual cortex (Ferster 1986; Ts'o, Gilbert, and Wiesel 1986; Martin 1988). The factors of N_E and N_I are introduced in order to facilitate the analysis of the size of the inputs from the above three sources in a large, highly connected network. It is assumed that each neuron is connected to a significant fraction of neurons of both subpopulations. Thus, with the above normalization, the *total* inputs $I^{\alpha\beta}$ from each of the populations are proportional in scale to the functions $J^{\alpha\beta}$ (for a detailed discussion of this scaling, see Hansel and Sompolinsky 1996; for alternative scaling of connections in large networks, see Van Vreeswijk and Sompolinsky 1996).

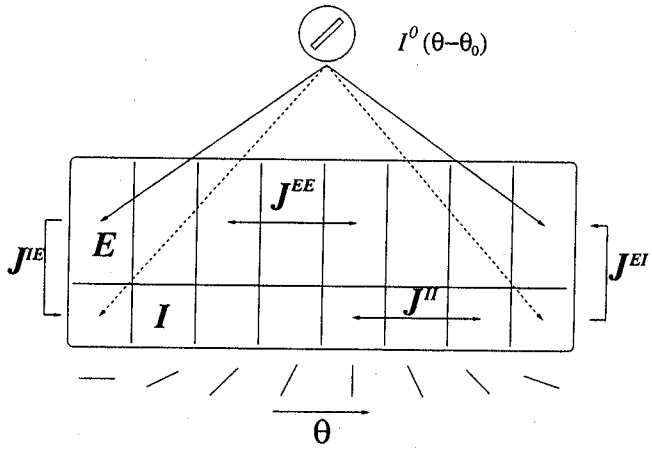

Figure 13.1
Architecture of the network.

To model the information carried by the stimulus about the external features, the input to the neuron θ of type α is taken to be of the form $I^{\alpha 0}(\theta - \theta_0)$, where θ_0 denotes the feature for which the external input is maximal. Thus θ_0 represents the feature value selected by the external input, or simply the stimulus feature. The network architecture is shown in figure 13.1.

A simple model of the interactions and of the external stimulus is given by retaining only the first Fourier components of their feature dependence. Thus

$$J^{\alpha\beta}(\theta - \theta') = J_0^{\alpha\beta} + J_2 \cos(2(\theta - \theta')), \tag{13.2}$$

where $J_0^{\alpha E} \geq J_2^{\alpha E} \geq 0$ and $J_0^{\alpha I} \leq J_2^{\alpha I} \leq 0$. These inequalities are consistent with the above assumption that both excitatory and inhibitory interactions are maximal for neurons with similar PFs. Likewise,

$$I^{\alpha 0}(\theta - \theta_0) = C_\alpha(1 - \varepsilon + \varepsilon \cos(2(\theta - \theta_0))), \quad 0 \leq \varepsilon \leq 0.5. \tag{13.3}$$

The above functions are depicted in figure 13.2A and figure 13.2B. The parameters C_α are assumed to be positive. They denote the maximal amplitude of the external inputs to the two populations. We will refer to them simply as the "stimulus intensity." The parameter ε measures the degree of modulation of the input to the cortical neurons. In the limit $\varepsilon = 0.5$, the external input to neurons farthest away from the stimulus feature, namely, neurons with $\theta = \theta_0 \pm \pi/2$, is zero. For $\varepsilon = 0$, the external input to all neurons in the same population is identical. We will refer to ε as the "stimulus tuning;" it is important to note that this parameter is determined both by the degree of tuning of the sensory stimulus itself and by the organization of

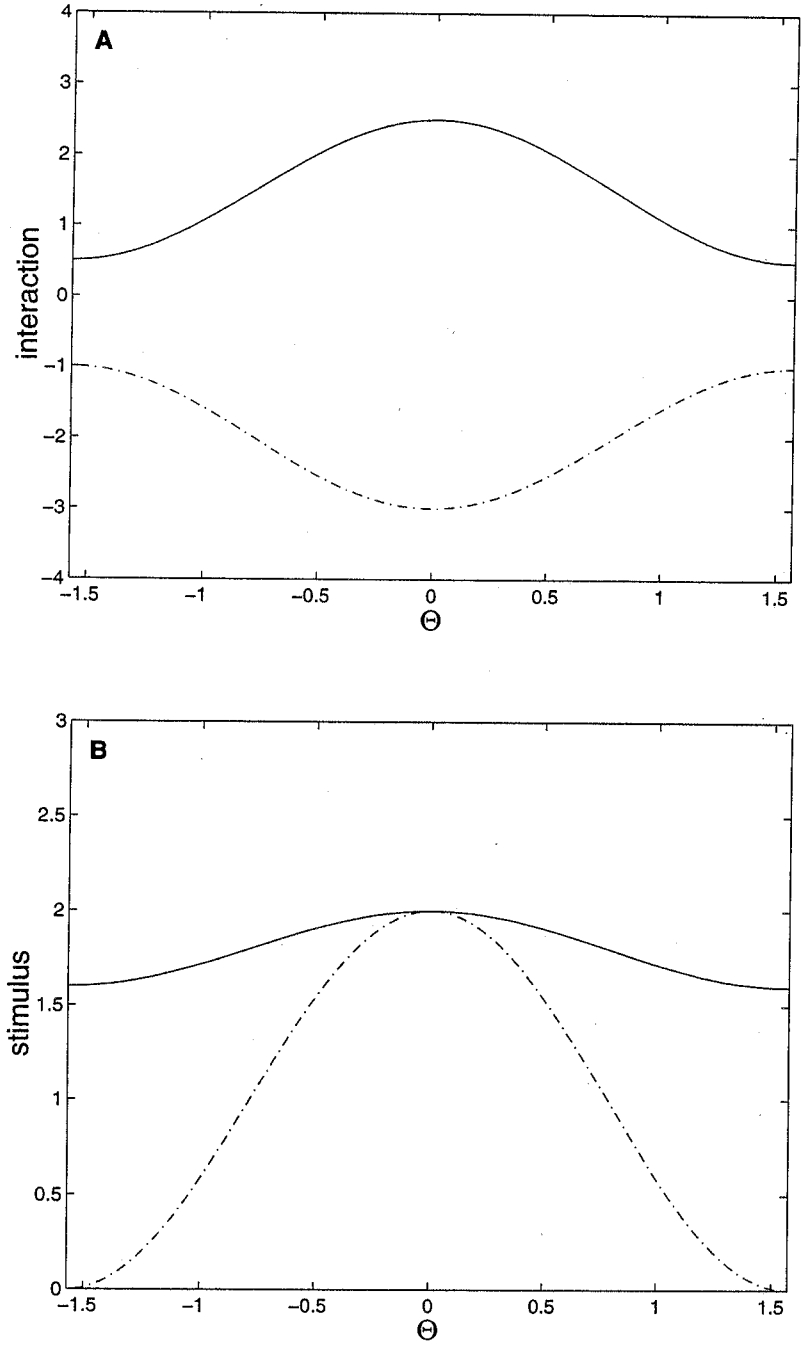

Figure 13.2
(A) Interactions as given in eq. 13.2. Solid line: excitatory interaction, with $J_0^{\alpha E} = 1.5$ and $J_2^{\alpha E} = 1$; dash-dotted line: inhibitory interaction, with $J_0^{\alpha I} = -2$ and $J_2^{\alpha I} = -1$. (B) Example of a stimulus given by eq. 13.3, with $C_\alpha = 2$. Solid line: $\varepsilon = 0.1$; dash-dotted line $\varepsilon = 0.5$.

the afferents to individual cortical neurons. In general, C_α, ε, and θ_0 may be time-dependent. To complete the model, we specify the dynamics of the network below.

13.2.2 Network Dynamics

Our theoretical study will be based on a relatively simple rate model in which the highly nonlinear dynamics of spiking neurons is replaced by smooth equations which describe the temporal evolution of the neuronal activities. These activities are smooth functions of time and represent the rate of firing averaged over short periods of time. In the present context, the rate (or simply the activity) of a neuron (α, θ) at time t is represented by the continuous functions of time, $m_\alpha(\theta, t)$, where as before $\alpha = E, I$, for excitatory and inhibitory neurons, respectively. It is convenient to normalize the rates by appropriate saturation levels so that $0 \leq m^\alpha(\theta, t) \leq 1$. Thus, $m^\alpha = 1$ represents firing rate of the order of 1 kHz. The rate variables are assumed to obey the following dynamic equations (Wilson and Cowan 1972; Ginzburg and Sompolinsky 1994; Ben-Yishai, Hansel, and Sompolinsky 1997):

$$\tau_0 \frac{d}{dt} m^\alpha(\theta, t) = -m^\alpha(\theta, t) + G(I^\alpha(\theta, t) - T_\alpha), \quad \alpha = E, I, \tag{13.4}$$

where τ_0 is a microscopic characteristic time assumed to be of the order of a few milliseconds. The quantities $I^\alpha(\theta, t)$ are the total synaptic inputs to the neuron $\alpha\theta$ (see eq. 13.1). The two network contributions to $I^\alpha(\theta, t)$ are of the form

$$I^{\alpha\beta}(\theta, t) = \int_{-\pi/2}^{+\pi/2} \frac{d\theta'}{\pi} J^{\alpha\beta}(\theta - \theta') m^\beta(\theta', t), \quad \beta = E, I. \tag{13.5}$$

Here we have used a mean field description, valid for large networks, according to which the activity profiles $m^\alpha(\theta, t)$ are continuous functions of θ. The parameters T_α are the neuronal thresholds. For the nonlinear gain function $G(I)$, we will adopt the simple semilinear form

$$G(I) = \begin{cases} 0 & I < 0 \\ I & 0 < I < 1 \\ 1 & I > 1. \end{cases} \tag{13.6}$$

Furthermore, we will demand that the stable state of the network is such that all the neurons are far from their saturation level. Therefore in practice the only nonlinearity we will consider is a threshold nonlinearity,

$$G(I) = [I]_+, \tag{13.7}$$

where $[X]_+ = X$ for $X > 0$, and zero otherwise.

In the case of time-independent external inputs, the dynamics of the rate model may converge to a fixed point. The fixed point equations are

$$m^{\alpha}(\theta) = [I^{\alpha}(\theta) - T_{\alpha}]_{+}, \quad \alpha = E, I, \tag{13.8}$$

where $I^{\alpha}(\theta)$ depends on the network activity profiles $m^{\alpha}(\theta)$ through

$$I^{\alpha}(\theta) = \sum_{\beta=E,I} \int_{-\pi/2}^{+\pi/2} \frac{d\theta'}{\pi} J^{\alpha\beta}(\theta - \theta') m^{\beta}(\theta') + I^{\alpha 0}(\theta - \theta_0). \tag{13.9}$$

If we linearize eq. 13.4 with respect to a small perturbation near the above fixed point, we find that the criterion of the linear stability of the fixed point is that all the eigenvalues of the stability matrix

$$M_{\alpha\beta}(\theta, \theta') = -\delta(\theta - \theta')\delta_{\alpha\beta} + \Theta(I_{\alpha}(\theta)) J^{\alpha\beta}(\theta - \theta') \tag{13.10}$$

have negative real parts. The function $\Theta(x)$ is the step function, that is, $\Theta(x) = 1$, for $x > 0$, and zero otherwise.

12.3 One-Population Rate Model

The solution of the above two-population rate model is discussed in detail in Ben-Yishai, Hansel, and Sompolinsky (1997). Here we will study a simpler model, in which the excitatory and the inhibitory populations are collapsed into a single equivalent population. This reduces substantially the number of parameters and greatly facilitates the analysis of the system behavior (the justification of this reduction will be discussed in section 13.7). The one population model is described in terms of a single rate variable $m(\theta, t)$ which represents the activity of the population of neurons in the column θ at time t. The rate dynamics are defined by

$$\tau_0 \frac{d}{dt} m(\theta, t) = -m(\theta, t) + [I(\theta, t) - T]_{+}, \tag{13.11}$$

where

$$I(\theta, t) = \int_{-\pi/2}^{+\pi/2} \frac{d\theta'}{\pi} J(\theta - \theta') m(\theta', t) + I^{0}(\theta - \theta_0) \tag{13.12}$$

and T is the neuronal threshold.

Adopting the additional simplification of retaining only the first two Fourier components in the interaction and external input spatial dependencies as in eqs. 13.2

and 13.3, we have

$$J(\theta - \theta') = J_0 + J_2 \cos(2(\theta - \theta')), \quad J_2 \geq 0, -J_0 \tag{13.13}$$

and

$$I^0(\theta - \theta_0) = C(1 - \varepsilon + \varepsilon \cos(2(\theta - \theta_0))). \tag{13.14}$$

Substituting eqs. 13.13 and 13.14 into eq. 13.12 yields

$$I(\theta, t) = C(1 - \varepsilon) + J_0 r_0(t) + C\varepsilon \cos(2(\theta - \theta_0)) + J_2 r_2(t) \cos(2(\theta - \Psi(t))), \tag{13.15}$$

where

$$r_0(t) = \int_{-\pi/2}^{+\pi/2} \frac{d\theta}{\pi} m(\theta, t) \tag{13.16}$$

$$r_2(t) = \int_{-\pi/2}^{+\pi/2} \frac{d\theta}{\pi} m(\theta, t) \exp(2i(\theta - \Psi(t))). \tag{13.17}$$

The phase $\Psi(t)$ is defined by the requirement that $r_2(t)$ is a nonnegative real number. The quantities $r_0(t)$, $r_2(t)$, and $\Psi(t)$ are global measures of the activity profiles and are called the "order parameters" of the network. The first-order parameter r_0 measures the activity of the neurons averaged over the entire network. The second-order parameter $r_2(t)$ measures the degree of "spatial modulation" in the activity profile. The complex number $r_2(t) \exp(2i\Psi(t))$ represents a vector in two dimensions, which corresponds to the *population vector* of the system, evaluated by summing unit vectors pointed in the PFs of the neurons, weighted by their instantaneous activities (Georgopoulos, Taira, and Lukashin 1993; Schwartz 1993). The phase $\Psi(t)$ denotes the angle of the population vector and r_2 denotes its length, that is, the strength of the spatial modulation of the population. From a functional point of view, $\Psi(t)$ may represent the population coding of the stimulus feature (Seung and Sompolinsky 1993).

Fourier transforming of eq. 13.11 yields self-consistent equations for the temporal evolution of the order parameters, which in turn determines the dynamics of $m(\theta, t)$ (these equations are derived in chapter appendix A). In the following we study the properties of the fixed-point solutions. We first assume that, at the fixed point, the population profile $m(\theta)$ is centered at the peak of the external input, that is, at $\theta = \theta_0$, hence

$$\Psi = \theta_0. \tag{13.18}$$

Substituting eq. 13.18 in eq. 13.15, we observe that the fixed-point solution for eq. 13.11 has the form

$$m(\theta) = M(\theta - \theta_0), \tag{13.19}$$

where

$$M(\theta) = [I_0 + I_2 \cos(2\theta)]_+. \tag{13.20}$$

The coefficients I_0 and I_2 are

$$I_0 = C(1 - \varepsilon) + J_0 r_0 - T \tag{13.21a}$$

$$I_2 = C\varepsilon + J_2 r_2. \tag{13.21b}$$

Eq. 13.20 shows that eq. 13.18 is indeed self-consistent. The fixed-point values of the r_0 and r_2 are given by the self-consistent equations

$$r_0 = \int_{-\pi/2}^{+\pi/2} \frac{d\theta}{\pi} M(\theta) \tag{13.22}$$

$$r_2 = \int_{-\pi/2}^{+\pi/2} \frac{d\theta}{\pi} M(\theta) \cos(2\theta), \tag{13.23}$$

which will be analyzed below. An interesting quantity is the network gain, G, defined as the ratio between the activity of the maximally active neuron and the stimulus intensity relative to threshold:

$$G \equiv \frac{M(0)}{C - T}. \tag{13.24}$$

Note that, by definition, $G = 1$ for an isolated neuron.

The stability of the above fixed point is determined by the following equation for the linear perturbation $\delta m(\theta, t) = m(\theta, t) - m(\theta)$:

$$\tau_0 \frac{d}{dt} \delta m(\theta, t) = -\delta m(\theta, t) + \Theta(m(\theta))(J_0 \delta r_0(t) + J_2 \delta(\cos 2(\theta - \Psi(t)) r_2(t))). \tag{13.25}$$

As usual, stability requires that the solutions for $\delta m(\theta, t)$ decay to zero. (This stability analysis can also be reduced to the study of the stability of the order parameters, as described in chapter appendix B.)

13.4 Stationary Activity Profiles

To solve eqs. 13.20–13.23, we have to distinguish between broad and narrow profiles. We say that the activity profile is "broad" when all the neurons are above threshold for all stimulus angles, that is, $M(\theta)$ is positive, for all θ. Conversely, a

"narrow" profile is characterized by $M(\theta)$ that vanishes at and beyond a certain angle θ_C. Of course, whether the profile is broad or narrow depends both on the stimulus inhomogeneity and on the cortical interaction parameters, as will be shown below. Note that $m(\theta)$'s being a function of the difference between θ and θ_0 implies that the form of the activity profile $M(\theta)$ is identical to the form of the output tuning curve of a single neuron. Thus a narrow (broad) profile corresponds to a narrow (broad) output tuning curve.

13.4.1 Broad Activity Profile

We first consider the relatively simple case of a broad $M(\theta)$, where all the neurons are above threshold. Thus eq. 13.20 simply reads

$$M(\theta) = I_0 + I_2 \cos(2\theta). \tag{13.26}$$

Substituting this expression in eqs. 13.22–13.23 yields $r_0 = I_0$; $r_2 = I_2/2$. Substituting in eqs. 13.21a–13.21b results in

$$r_0 = \frac{C(1-\varepsilon) - T}{1 - J_0} \tag{13.27}$$

$$r_2 = \frac{C\varepsilon}{1 - \frac{1}{2}J_2}. \tag{13.28}$$

In the case of a homogeneous input, $\varepsilon = 0$, the above solution reduces to a homogeneous state:

$$M(\theta) = \frac{C - T}{1 - J_0}, \quad \varepsilon = 0. \tag{13.29}$$

For $\varepsilon > 0$, the gain is

$$G = \frac{1 - \Upsilon}{1 - J_0} + \frac{2\Upsilon}{1 - \frac{1}{2}J_2}, \tag{13.30}$$

where the *effective stimulus tuning* is defined as

$$\Upsilon = \frac{\varepsilon C}{C - T} \tag{13.31}$$

As expected, positive feedback generated by positive J_0 or J_2 enhances the system's gain, whereas negative feedback suppresses it. As we will see below, the parameter Υ is an important measure of stimulus tuning: it takes into account the potential enhancement of the tuning of cortical neuron activity by the effect of its threshold.

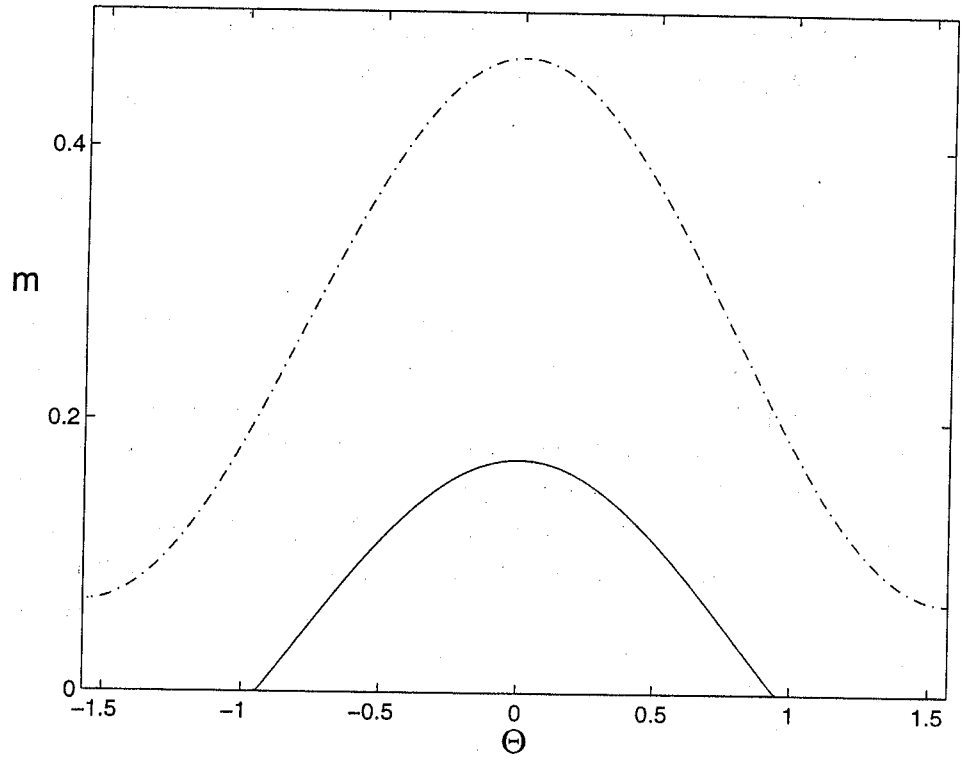

Figure 13.3
Activity profile in the one-population rate model for $J_0 = -2$ and $J_2 = 0$. The tuning of the input is $\varepsilon = 0.1$. The profile of activity is broad for a contrast $C = 2$ (dash-dotted line). For a lower contrast, here $C = 1.3$ (solid line) the profile is narrow.

When the stimulus intensity is close to threshold, a weak stimulus tuning will cause a relatively narrow output tuning because the neuron will be active only if it is maximally stimulated. It should be noted, however, that Υ is a single-neuron property. It does not take into account the potential modification of the threshold by the cortical network. An example of a broad profile is shown in figure 13.3.

Eqs. 13.26–13.28 are a self-consistent solution of eq. 13.20, provided that the gain given by eq. 13.30 is positive. This depends on the value of Υ. For sufficiently large values of Υ, G becomes negative and the broad solution is not valid any more. In addition, one has to consider the stability of this solution. The stability analysis is performed by Fourier transforming eq. 13.25 (taking into account that here $\Theta(m(\theta)) = 1$, for all θ), yielding

$$\tau_0 \frac{d}{dt}\delta r_0(t) = -(1 - J_0)\delta r_0(t) \tag{13.32}$$

$$\tau_0 \frac{d}{dt}\delta r_2(t) = -\left(1 - \frac{J_2}{2}\right)\delta r_2(t). \tag{13.33}$$

(See chapter appendix B for a full treatment of the stability analysis.) These equations define two stability conditions that are independent of Υ:

$$J_0 < 1 \tag{13.34}$$

and

$$J_2 < 2. \tag{13.35}$$

At $J_0 = 1$, the system undergoes an *amplitude instability* characterized by the divergence of the activity levels of all neurons in the network. Indeed, if we add the saturation nonlinearity of eq. 13.6, we find that when $J_0 = 1$, all the neurons fire at saturation level. The instability at $J_2 = 2$ signals a *spatial instability*, where the system prefers a narrowly tuned state over the broadly tuned one, even when Υ is zero. In other words, when the spatial modulation of the cortical feedback is large, even a small inhomogeneous perturbation (generated by a small Υ, or even a nonzero initial value of r_2, with $\Upsilon = 0$) will grow due to cortical feedback, and will destroy the underlying homogeneous state. The resultant state is described below.

13.4.2 Narrow Activity Profile

We have defined above an activity profile as *narrowly tuned* if there exists an angle θ_C such that $M(\theta)$ vanishes for $|\theta| \geq \theta_C$. In this case, eq. 13.20 is no more linear. It can be written as

$$M(\theta) = I_2[\cos(2\theta) - \cos(2\theta_C)]_+, \tag{13.36}$$

where

$$\cos(2\theta_C) = \frac{-I_0}{I_2}. \tag{13.37}$$

The angle θ_C denotes the width of the tuning curve. Substituting in eqs. 13.22–13.23 yields, after some algebra, the following self-consistent equation for θ_C:

$$1 - \frac{1}{\Upsilon} = \frac{J_0 f_0(\theta_C) + \cos(2\theta_C)}{1 - J_2 f_2(\theta_C)}, \tag{13.38}$$

where

$$f_0(\theta_C) = \frac{1}{\pi}(\sin(2\theta_C) - 2\theta_C \cos(2\theta_C)) \tag{13.39}$$

$$f_2(\theta_C) = \frac{1}{\pi}\left(\theta_C - \frac{1}{4}\sin(4\theta_C)\right). \tag{13.40}$$

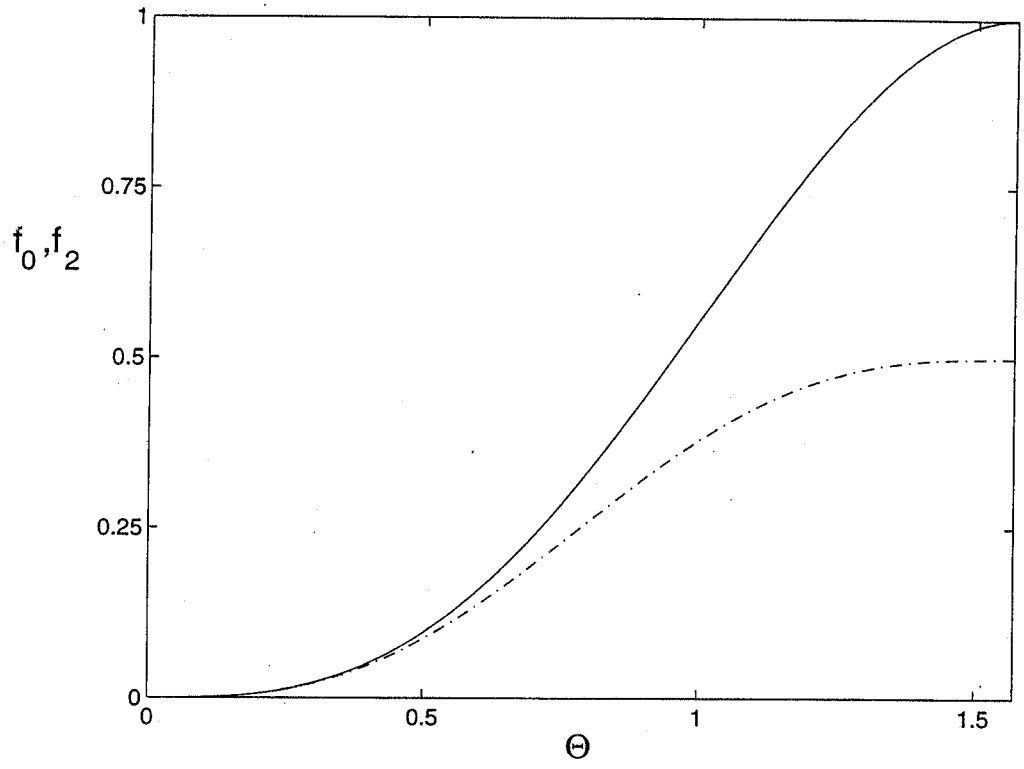

Figure 13.4
Function $f_0(\theta)$ (solid line) and $f_2(\theta)$ (dashed-dotted line).

These functions are plotted in figure 13.4. The gain of the network

$$G = \frac{I_2(1 - \cos(2\theta_C))}{C - T} \tag{13.41}$$

is given by

$$G = \Upsilon\left(\frac{1 - \cos(2\theta_C)}{1 - J_2 f_2(\theta_C)}\right). \tag{13.42}$$

These equations (derived in chapter appendix A) are a valid solution for the fixed point provided G is positive and eq. 13.38 has a solution; otherwise, the only solution is a broadly tuned one, as described above. Finally, the stability of this solution has to be determined by linearizing the dynamics around this fixed point (the resultant stability conditions are derived in chapter appendix B). An example of a narrow profile is shown in figure 13.3. We discuss below the interaction parameters where the broad or the narrow solutions are the stable states of the system.

13.4.3 Weakly Modulated Cortical Interactions

When the tuning of the input is large, that is, $\Upsilon \gg 1$, the cortical interactions may have little effect on the shape of the activity profile. On the other hand, when the stimulus tuning is weak, the cortical interactions may play a large role in the emergent network tuning. Thus a convenient way to characterize the effect of the cortical interactions is to calculate the influence on the critical value of Υ, denoted as Υ_c, below which the system has a broad activity profile. According to our analysis above, we suspect that Υ_c is positive for $J_2 < 2$, whereas $\Upsilon_c = 0$ for $J_2 > 2$. The role of J_0 is different: it may affect the value of Υ_c, but it will not drive it to *zero* if $J_2 < 2$. In addition, the value of J_0 may affect the overall stability of the system. A large positive value of J_0 signals strong positive feedback, which causes an instability of the network state. The above qualitative considerations are borne out by our detailed results below. We first consider the regime of weakly modulated interactions defined by

$$J_2 < 2, \quad J_0 < 1. \tag{13.43}$$

Afferent Mechanism of Feature Selectivity The classical model of feature selectivity assumes that the selectivity is generated by the spatial organization of the afferent input to the cortical neurons. In the context of our model, this implies that Υ is large and that the contribution of the cortical interactions is not essential, namely,

$$J_0, \quad J_2 \approx 0. \tag{13.44}$$

In this case, the narrow profile described by eq. 13.20 reduces to

$$M(\theta) = \varepsilon C[\cos(2\theta) - \cos(2\theta_C)]_+, \tag{13.45}$$

where θ_C is

$$\theta_C = \frac{1}{2}\arccos(1 - \Upsilon^{-1}), \quad \Upsilon > \Upsilon_c. \tag{13.46}$$

The lowest value of Υ for which this solution exists is

$$\Upsilon_c = \frac{1}{2}. \tag{13.47}$$

For $\Upsilon < \Upsilon_c$, the system is in a broadly tuned state, where

$$M(\theta) = C(1 - \varepsilon) - T + \varepsilon C \cos(2(\theta - \theta_0)), \quad \text{for } \textit{all } \theta \tag{13.48}$$

These results are shown in figure 13.5. Finally, in the absence of cortical interactions, the gain of the system is the same as that of a single neuron, namely, $G = 1$.

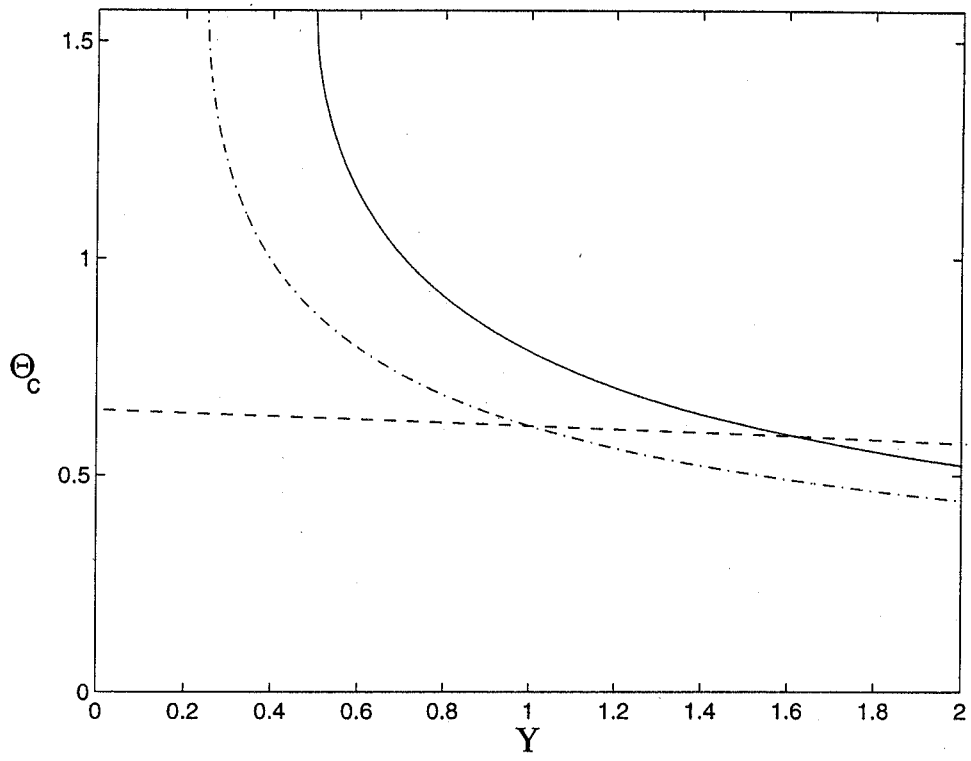

Figure 13.5
Width of the tuning curve, Θ_c, as a function of Υ. Solid line; afferent mechanism; dash-dotted line: uniform cortical inhibition, $J_0 = -2$; dashed line: marginal phase, $J_0 = -2$ and $J_2 = 6$.

Uniform Cortical Inhibition The previous feedforward scenario has an obvious drawback. If the input tuning ε is smaller than $1/2$, sharply tuned profile exists only if the intensity is near the single-neuron threshold. A stimulus with $\varepsilon < 1/2$ and a high intensity relative to T will necessarily generate broad profiles of activity. A simple mechanism for sharpening the tuning invokes global cortical inhibition. Within our model, this scenario corresponds to the parameter regime

$$J_0 = -|J_0| < 0, \quad J_2 \approx 0. \tag{13.49}$$

In the presence of this inhibition, the external input of each neuron has to overcome an effective threshold given by $\pi + |J_0|r_0$. This effective threshold increases linearly with r_0 and therefore also with C. Thus, even for $C \gg 1$ and small ε, the uniform inhibition can provide a sufficiently potent threshold to sharpen the tuning width. In particular, substituting eq. 13.49 in eq. 13.38 and noting that the maximal value of θ_C is $\pi/2$, we see that a narrow profile exists as long as Υ is bigger than

$$\Upsilon_c = \frac{1}{2 + |J_0|}. \tag{13.50}$$

The effect of J_0 on θ_C is shown in figure 13.5, which shows clearly that although the inhibition sharpens the orientation tuning, the value of θ_C depends strongly on Υ, hence on both C and ε. This highlights the fact that uniform inhibition is incapable of generating feature tuning on its own; it can only sharpen the tuning generated by the modulated input. Finally, from eq. 13.42 we have in the present case

$$G = \Upsilon(1 - \cos(2\theta_C)). \tag{13.51}$$

Because the cortical inhibition reduces θ_C, it suppresses the system's gain as expected.

General Case The effect of adding a positive J_2 is to sharpen the tuning of the network. As illustrated in figure 13.6, for fixed values of J_0, Υ_c decreases with J_2 until it vanishes at $J_2 = 2$. This indicates that for larger values of J_2, even when Υ is zero, the system's activity profile is narrow (see section 13.4.4).

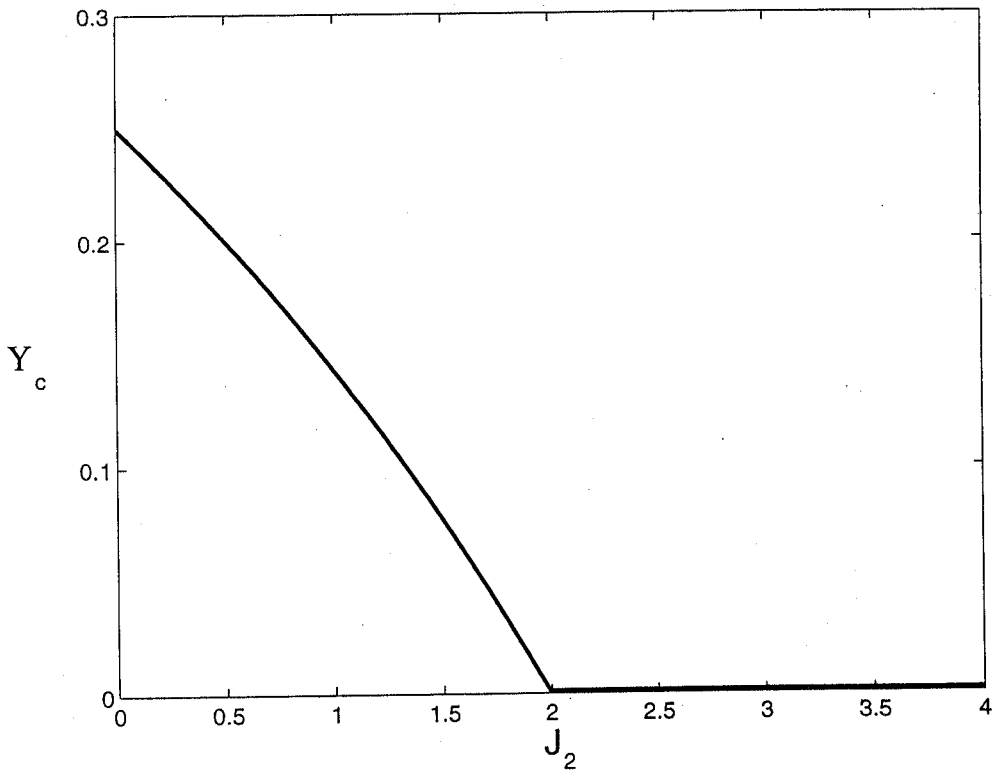

Figure 13.6
Υ_c as a function of the modulation J_2, for $J_0 = -2$.

13.4.4 Strongly Modulated Cortical Interactions

We now consider the parameter regime

$$J_2 > 2, \quad J_0 < J_C. \tag{13.52}$$

The upper bound on J_0, J_C, is a function of J_2 and Υ, as will be discussed below.

Homogeneous Input: Marginal Phase In section 13.4.3, we analyzed the case where the external input is the only source of modulation of the cortical activity. In this section, we consider the question: can a narrow activity profile be generated by spatially modulated cortical interactions even in the absence of tuning in the external input? To study this question, we assume here

$$J_2 > 0, \quad \varepsilon = 0. \tag{13.53}$$

According to our previous analysis, the homogeneous state, characterized by eq. 13.29 is unstable. It is also clear that if the system possess an additional, inhomogeneous solution, this solution must be narrowly tuned because a broadly tuned profile obeys linear dynamics that does not poses more than one fixed point. Indeed, inspection of eq. 13.20 reveals that, for $\varepsilon = 0$, solutions with a narrow activity profile exist for $J_2 > 2$. The general stable solution is of the form

$$m(\theta) = M(\theta - \Psi). \tag{13.54}$$

The angle Ψ, which determines the peak in the population activity profile, is arbitrary because the external input is homogeneous. This means that there is a continuum of stable states. All the states have identical feature-tuned activity profiles, although the peaks of their profiles differ in location. Such a situation is termed a *marginal phase*, which indicates that the system relaxes to a line of fixed points rather than to one or several isolated fixed points. A marginal phase represents *spontaneous symmetry breaking*, that is, spontaneously generated spatial modulation of the activity in the network, and arises because spatial modulation of the cortical interactions, if sufficiently strong, destabilizes the homogeneous state. The stable state of the network is one where the activity is concentrated in a limited spatial range.

The shape of the activity profile in the marginal phase is still given by eq. 13.36. As for the width of the profile, inspection of eq. 13.38 reveals that when $\Upsilon = 0, \theta_C$ is given by

$$J_2 f_2(\theta_C) = 1, \tag{13.55}$$

which has a solution for $J_2 > 2$ (see figure 13.4). The gain in this limit is given by

$$G = \frac{1 - \cos(2\theta_C)}{f_0(\theta_C)} \left(\frac{1}{J_C - J_0} \right) \tag{13.56}$$

and

$$J_C = -\frac{\cos(2\theta_C)}{f_0(\theta_C)}, \quad \Upsilon \to 0. \tag{13.57}$$

Eqs. 13.36, 13.41, and 13.56, together with eq. 13.55, which determines θ_C, complete the solution for the activity profile. These equations imply that the amplitude of the external input determines the overall level of activity in the system, although the shape of the activity profile, in particular its width, is determined by the degree of spatial modulation of the cortical interactions.

It is clear from eq. 13.56 that for the marginal state to exist, J_0 has to be smaller than J_C (this condition can be also derived from a stability analysis presented in chapter appendix B). When J_0 approaches J_C, the system undergoes an amplitude instability similar to the instability that occurs at $J_0 = 1$ for the homogeneous state and $J_2 < 2$ (see eq. 13.32). The phase diagram for the stability of the various states in the case of a homogeneous stimulus is depicted in figure 13.7.

Tuned Input We have considered a completely homogeneous input, for which the location of the peak of the activity profile is arbitrary. Because, however, we are primarily interested in how the system represents features present in external stimuli, we consider the solution of eqs. 13.36–13.42 in the parameter regime

$$0 < J_2 < 2, \quad \varepsilon > 0. \tag{13.58}$$

Solving eq. 13.38 shows that in most of this regime the tuning is largely independent of Υ, as illustrated in figure 13.5. This implies that the shape of the activity profile is determined essentially by the cortical interactions, eq. 13.55, and is barely affected by the presence of nonzero values of Υ. Thus the main effect of the inhomogeneity of the external input is to select among the continuum of possible states that state in which the peak in the activity matches the feature of the stimulus, that is

$$\Psi = \theta_0. \tag{13.59}$$

However, it will not greatly affect the shape of the tuning curve, as shown in figure 13.8. An exception is the case of low-intensity stimuli, characterized by C close to threshold T, that is, a large Υ. Once the single-neuron thresholding effect becomes

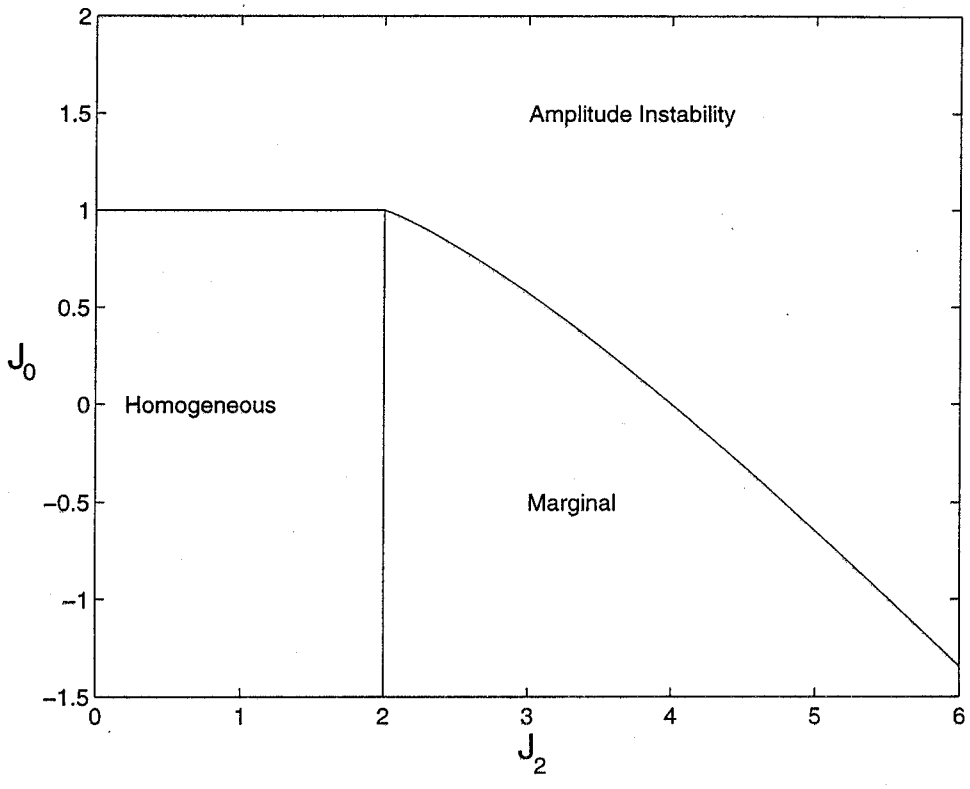

Figure 13.7
Phase diagram of the one-population rate model for $\varepsilon = 0$.

dominant, it sharpens the tuning curve beyond the sharpening provided by the cortical mechanisms. Another regime where the value of Υ is important is near the amplitude instability. This is because the critical value of J_0, J_C, depends on both J_2 and Υ, as shown in the phase diagram (figure 13.7). As Υ increases, the value of J_C decreses, expanding the regime where the fixed-point state is table.

Finally, we would like to point out the two main features that make the one-population model defined by eqs. 13.11–13.13 particularly simple. First, because the synaptic interaction, eq. 13.13, consists of only two Fourier components, the full dynamics can be reduced to a set of self-consistent equations involving a small number of order parameters, in our case, r_0, r_2, and Ψ. Second, as a consequence of the choice of threshold linear gain function, the dynamic equations in the regime of active population are linear equation. The only nonlinearity is the self-consistent equation for θ_C that results from matching the boundary between the active and quiescent populations.

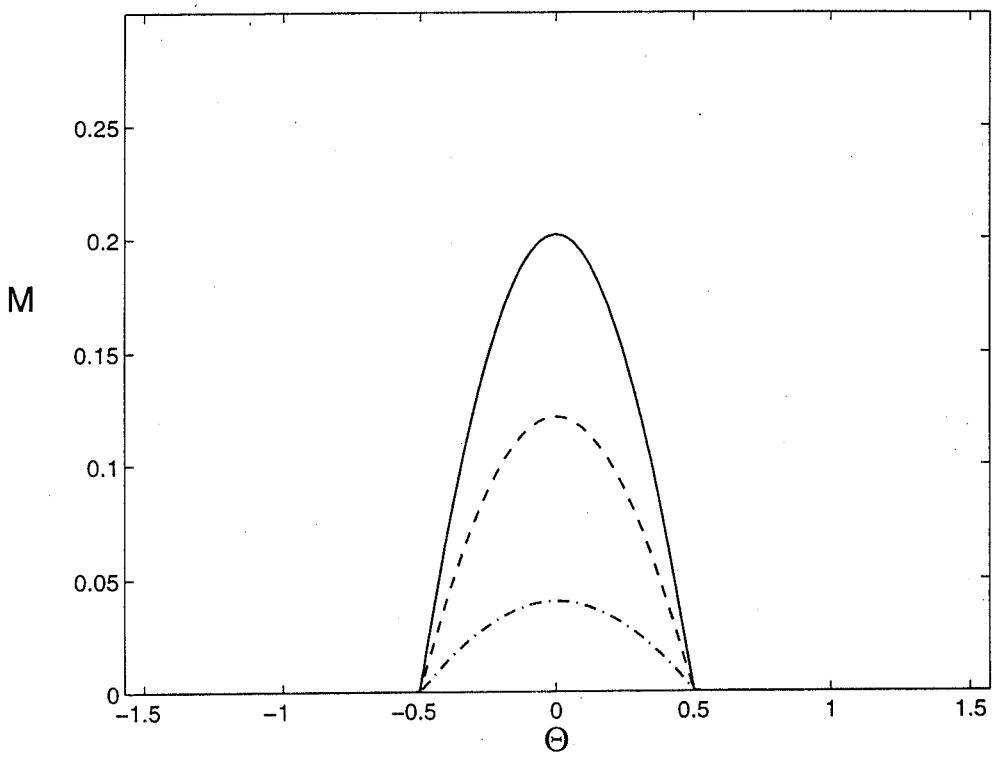

Figure 13.8
Activity profile of the one-population rate model in response to an homogeneous external input for different values of the intensity. $J_0 = -17.2$, $J_2 = 11.2$. Sold line: $C = 1.5$; dashed line: $C = 1.3$; dash-dotted line: $C = 1.1$.

13.5 Moving Activity Profiles

13.5.1 Response to Changing Stimulus Feature

Thus far, we have discussed the steady-state response to the onset of a stimulus with a time-independent feature value, θ_0. One of the most important consequences of the existence of the marginal phase is the dynamics of the system's response to perturbations. Consider the case where the system reaches a stable state located at the peak of weakly tuned input, and a weak transient perturbation is applied on it. Qualitatively, we expect that if the perturbation puts the system momentarily in a state unlike one of the attractor states, the system will quickly relax to the nearest stable profile. On the other hand, if the perturbation puts the system in a different state on the attractor, the system will relax to the original state, that is, the profile will move to its original location relatively slowly, and it will strongly depend on Υ, which represents the restoring force toward the original state. Indeed, for small perturbations, the

relaxation times are the inverse of the eigenvalues of the stability matrix of the marginal phase (calculated in chapter appendix B). Eqs. 13.B15, 13.B16, and 13.B21 imply that whereas the relaxation times of the shape of the profile, which involves perturbation of r_0 and r_2, are short even in the marginal phase, the relaxation time of the perturbation to the position of the profile, namely, Ψ, is long and diverges in the limit of $\Upsilon \to 0$.

The slow dynamics of the marginal phase is manifest also in the response of the system to a time-dependent stimulus where θ_0 changes with time. In the present notation, such a stimulus is parametrized as

$$I^0(\theta, t) = I^0(\theta - \theta_0(t)) = C(1 - \varepsilon + \varepsilon \cos(2(\theta - \theta_0(t))). \tag{13.60}$$

The dynamics of the network is described by eqs. 13.11–13.15, with time-dependent θ_0. The nature of their solution depends on the interaction parameters as well as on the stimulus-effective tuning parameter Υ. In general, if Υ is large, the response of the network may be dominated by the single-neuron dynamics, and the feedback effects will be minor. Here we will focus on the case of a *weakly tuned* input that *varies slowly* with time, where the network behavior may be quite different from that of an isolated neuron. In this regime, the dynamics of the network can be reduced to a simplified *phase model*, similar in some respects to phase descriptions of neuronal oscillatory systems. Our assumptions about the stimulus are formally expressed as

$$\left| \tau_0 \frac{d\theta_0}{dt} \right| = O(\Upsilon) \ll 1. \tag{13.61}$$

Under these conditions, after a long time compared to τ_0, the *shape* of the activity profile of the network becomes almost stationary and has the same form as that for a constant θ_0 and low Υ. The main effect of the motion of the stimulus is to initiate a translation of the activity profile across the network. Thus

$$m(\theta, t) = M(\theta - \Psi(t)), \tag{13.62}$$

where $M(\theta)$ has the same shape as in the stationary case at low Υ, which is given by eqs. 13.36, 13.56, and 13.55. The motion of the profile is conveniently described in terms of the difference between the instantaneous locations of the activity profile and the stimulus feature:

$$\Delta(t) = \Psi(t) - \theta_0(t). \tag{13.63}$$

In chapter appendix A, we show that, to leading order in ε, $\Delta(t)$ obeys the following equation:

$$\frac{d\Delta(t)}{dt} = -\frac{d\theta_0}{dt} + V_C \sin(2\Delta(t)), \tag{13.64}$$

where

$$\tau_0 V_C = \frac{\Upsilon}{2} f_0(\theta_C)(J_C - J_0) = \frac{\Upsilon(1 - \cos(2\theta_C))}{2G} \tag{13.65}$$

and where J_C is given in eq. 13.57. Note that $1/V_C$ is proportional to the large relaxation time of perturbations of Ψ, as seen in eq. 13.B21. We now discuss two applications of this equation.

Response to Sudden Change in Stimulus Feature–Virtual Rotation Consider the case where a stimulus with a feature value θ_1 is presented in the receptive field of the cells for a time sufficiently long that a stationary response to the stimulus that a stationary response to the stimulus has developed. Then at time $t = 0$ the stimulus feature is suddenly changed to the value θ_2. How will the cells respond to this change? We consider here separately the regimes of weak and strong cortical modulation.

To illustrate the transient response in the weak modulation regime, we consider the case of zero modulation of the cortical interactions, namely, $J_2 = 0$. In this case the evolution in time of $m(\theta, t)$ is given, according to eq. 13.11, by

$$\tau_0 \frac{d}{dt} m(\theta, t) = -m(\theta) + [I^0(\theta - \theta_2) + J_0 r_0 - T]_+, \quad t > 0, \tag{13.66}$$

where I^0 is the external input (eq. 13.14) corresponding to the second stimulus. This equation has to be solved with the initial condition $m(\theta, t = 0) = [I^0(\theta - \theta_1) - T]_+$. As will be shown below, the mean network activity r_0 is constant in time, hence the solution to eq. 13.66 is simply

$$m(\theta, t) = M(\theta - \theta_1)e^{-t/\tau_0} + M(\theta - \theta_2)(1 - e^{-t/\tau_0}), \quad t \geq 0, \tag{13.67}$$

where $M(\theta)$ is the stationary profile under constant stimulus with $\theta_0 = 0$. Thus the initial activity profile decays while the final one grows in amplitude, as shown in figure 13.9A, while intermediate columns remain inactive throughout this response. Note that r_0 indeed remains constant in time, as can be verified by spatial averaging of eq. 13.67. Thus the change in the stimulus redistributes the activity among the neurons within the network without affecting the mean activity level. For this reason, the network feedback $J_0 r_0$ does not modify the time constant associated with the buildup of activity around θ_2. Indeed, according to eq. 13.67, this time constant is the single-neuron time constant, τ_0.

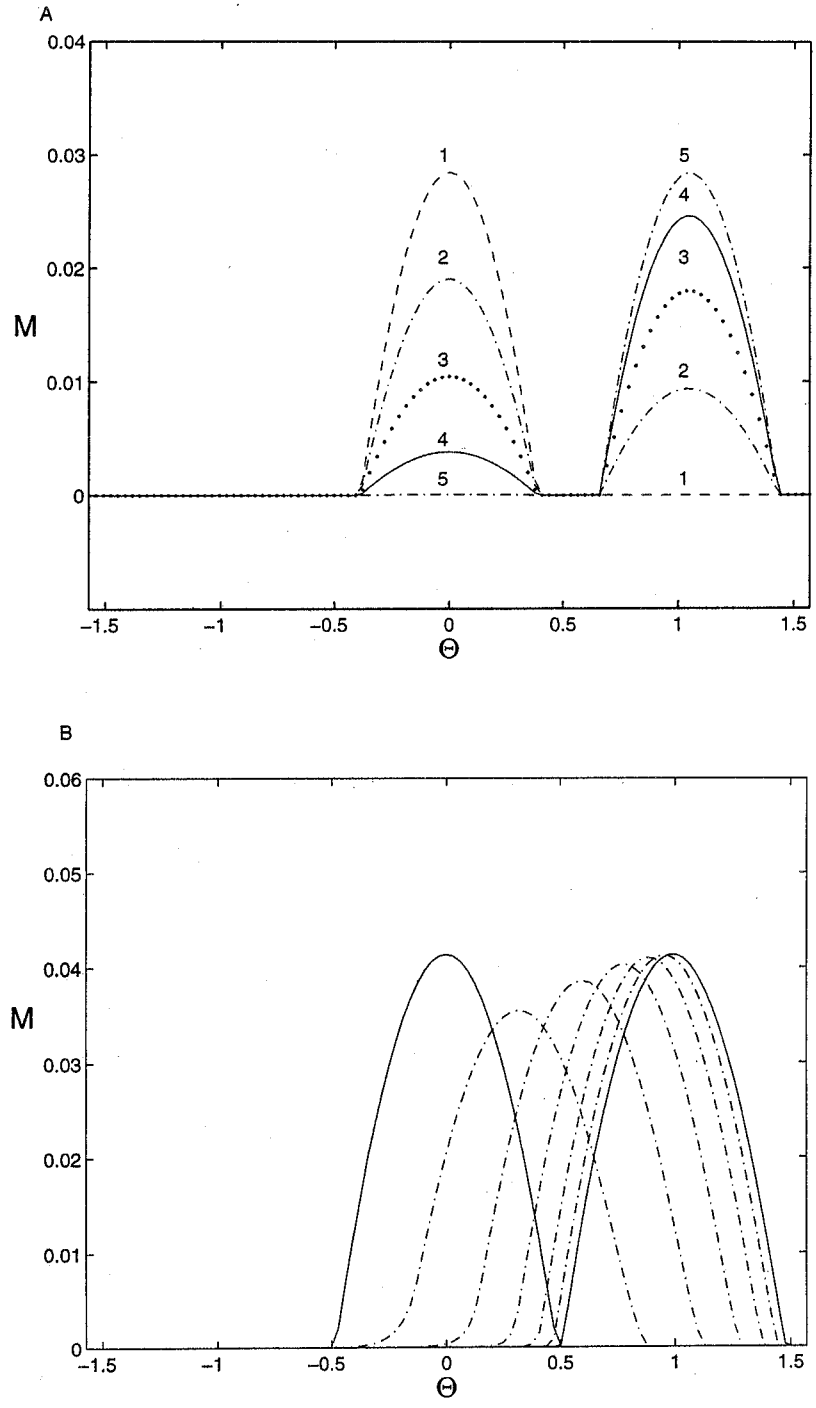

Figure 13.9
Evolution of the neuronal activity in response to a change in the stimulus orientation from an initial value $\theta_1 = 0^0$ to $\Theta_2 = 60^0$. The change occurs at $t = 0$. (A) Afferent mechanism with uniform inhibition. Parameters: $J_0 = -15.5$, $C = 1.1$, $\varepsilon = 0.5$. Times (units of τ_0): 0, 0.5, 1, 2, 6 (lines 1–5, respectively). (B) Virtual rotation in the marginal phase. The activity profile is moving toward θ_2. Parameters: $J_0 = -17.2$, $J_2 = 11.2$, $\varepsilon = 0.05$, $C = 2$. Times (left to right): 0 to $35\tau_0$ each $5\tau_0$.

We next consider the case of a cortical network with weakly tuned stimulus and strongly modulated interaction, where not only the mean activity but also the shape of the profile of the population activity changes very little with time. The main effect of the time evolution is to move the center of the profile until it matches the new stimulus feature θ_2. The evolution in time of the center of the activity profile is given by

$$\frac{d\Delta(t)}{dt} = -V_C \sin(2\Delta(t)), \quad \Delta(t=0) = \theta_1 - \theta_2, \tag{13.68}$$

where $\Delta(t) = \Psi(t) - \theta_0(t)$. Note that, for $t > 0$, $\Delta(t)$ denotes the center of the population profile relative to the instantaneous stimulus, here θ_2. The solution of this equation is

$$\Delta(t) = \arctan(A \exp(-2V_C t)), \tag{13.69}$$

where $A = \tan(\Delta(0))$. Figure 13.9B shows the full solution results of the network dynamics, for $\Upsilon = 0.1$. One sees that the changes in the shape of the activity profile are small and successive activation of the intermediate columns indeed occurs, as predicted by the phase model.

The above results mean that, at any given time t, the population activity is similar to what would occur if there were an external stimulus with a feature $\theta_0 = \Psi(t)$. Thus the temporal evolution of the cortical state corresponds to a virtual smooth change of an external stimulus with a velocity given by $d\Delta/dt$. This can therefore serve as a neural mechanism for various psychophysical phenomena related to apparent motion, including the well-studied phenomenon of "mental rotations" (Shepard and Metzler 1971). Note that if the difference between the initial and the final features equals $\pi/2$, eq. 13.68 predicts that the initial state with the peak located at θ_1 is a fixed point of the dynamics. This is, however, an unstable fixed point, so that slight perturbations will cause $\Psi(t)$ to grow toward $\theta_2 = \pi/2$ or decrease toward $-\theta_2 = -\pi/2$, depending on the nature of the perturbation. Finally, it should be noted that the result of eq. 13.68 is valid provided $V_C\tau_0 = O(\Upsilon) \ll 1$. Otherwise, the dynamics involve major deformations in the activity profile, which resembles the decay and growth pattern of eq. 13.67.

Locking to a Moving Stimulus Feature We now consider the response of the system to a stimulus with a feature value that changes smoothly with time, with a constant velocity,

$$\theta_0(t) = Vt. \tag{13.70}$$

If the system encodes the instantaneous stimulus orientation by the location of the population activity profile, then this profile should be able to follow the change in the stimulus, which raises the following question. Can the population activity profile lock to the input? If so, what is the range of input velocities for which such locking occurs? For a stimulus that varies on time scales comparable to single-cell time constants, the answers to the above questions may depend strongly on the details of the single-cell microscopic dynamics. When, however, the temporal variation of the stimulus is slow and the direct coupling of the population profile to the changing stimulus relatively weak, cortical cooperative effects may be the dominant factor in determing the locking properties. We therefore focus here on the case of a weakly tuned ($\Upsilon \ll 1$) and slow time-dependent input, $\tau_0 V = O(\Upsilon)$. In weakly modulated cortical interactions, the network's responses to the moving stimulus will be essentially linear, similar to the broad profile in the stationary case. The motion of the stimulus will induce a small time-dependent component of the neuron's activity. The situation is qualitatively different in the parameter regime of the marginal phase, where the tuning of the network will be sharp, hence the response to the stimulus is highly nonlinear. In this limit, the changing stimulus generates a motion of the whole activity profiles without greatly affecting their shape. Hence the state of the system is given approximately by an activity profile whose shape is stationary but whose center moves with time. The motion of the population activity center relative to the stimulus, $\Delta(t)$, is given by eq. 13.64, with $\theta_0(t)$ of eq. 13.70:

$$\frac{d\Delta(t)}{dt} = -V - V_C \sin(2\Delta(t)). \tag{13.71}$$

The nature of the solution of this equation depends on the stimulus velocity, V, relative to the intrinsic velocity constant, V_C.

SLOW STIMULUS ($V < V_C$) In this regime, eq. 13.71 has a stable fixed point:

$$\Delta = -\frac{1}{2}\arcsin(V/V_C). \tag{13.72}$$

This corresponds to a state in which the activity profile is locked to the stimulus and follows it with a constant phase lag. For $V \to V_C$, the phase lag between the excitatory population and the stimulus reaches $-\pi/4$. It should be emphasized that here, as opposed to the previous case, the locking is strong, involving the motion of a sharply tuned population profile. The positions of the population vectors and the stimulus in such a case are shown in figure 13.10A.

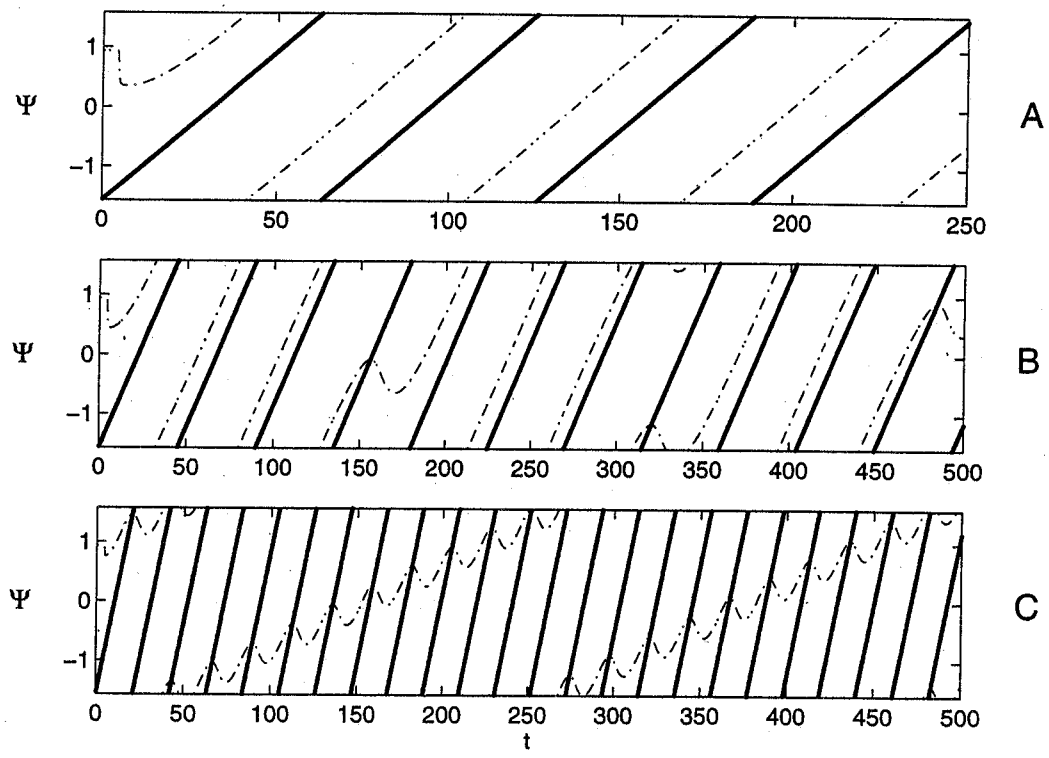

Figure 13.10
Response to a rotating stimulus in the marginal phase ($J_0 = -17.2, J_2 = 11.2, C = 1.1, \varepsilon = 0.05$). Bold lines are the feature of the stimulus, $\theta_0(t) = Vt$ as a function of time. Dash-dotted lines are the angle of the population vector. (A) Complete locking of the activity profile to the rotating stimulus at velocity $V = 0.05\,\text{rad}/\tau_0$. (B) Partial locking in the case $V = 0.07\,\text{rad}/\tau_0$. (C) No locking in the case $V = 0.15\,\text{rad}/\tau_0$.

FAST STIMULUS ($V > V_C$) In this regime, eq. 13.71 does not have a fixed-point solution, and the activity profile is not locked to the rotating stimulus. The solution of the phase equation yields

$$\Delta(t) = \arctan\left\{\frac{V_C}{V} + \frac{W}{V}\tan(V(t - t_0))\right\}, \tag{13.73}$$

where

$$\tau_0 W = \sqrt{V^2 - V_C^2} \tag{13.74}$$

and t_0 is determined by the initial condition $\Delta(0) = \Delta_0$. The phase Δ is periodic in time with a period $P = 2\pi/W$. Thus the rotation of the population vector is quasi-periodic, with $\Psi(t) = Vt - \Delta(t)$. The average velocity of the population vector rota-

tion is $V - W$, which is slower than the stimulus velocity, V. The behavior of $\Psi(t)$ for a value of V close to V_C is shown in figure 13.10B, and for a higher velocity in figure 13.10C. These results, obtained by numerical integration of the population dynamics, are in a good qualitative agreement with the predictions of the above phase equations, which are based on the limit of small ε and V.

13.5.2 Intrinsic Moving Profiles

Modeling Neuronal Adaptation One of the major limitations of the one-population model we have studied above is that, because of the symmetry of its connections (Hopfield 1984), it always settles into a stationary state when stimulated by a constant stimulus. Neuronal networks, on the other hand, quite often converge to an attractor that is not a fixed point, even when the stimulus is constant in time. A simple example is the appearance of stable temporal oscillations in the neuronal activity as a result of the network feedback (Wilson and Cowan 1972; Grannan, Kleinfeld, and Sompolinsky 1992). When the network architecture has spatial structure, as in our case, the time-dependent attractors are in general also spatially modulated. A simple class of such stable spatiotemporal patterns is a solution where a spatial activity profile rigidly moves across the network. Indeed, in the more complex architecture of a network comprising distinct excitatory and inhibitory populations, intrinsic moving profiles can appear, provided the internal spatial modulation of the inhibitory feedback is strong (this scenario has been studied in detail in Ben-Yishai, Hansel, and Sompolinsky 1997). Here we study a somewhat simpler scenario for generating such pattern, one that relies on neuronal adaptation, a ubiquitous phenomenon in excitatory cortical neurons (Connors, Gutnick, and Prince 1982; Connors and Gutnick 1990; Ahmed, Anderson, et al. 1994). Qualitatively, the movement of the activity profile is caused by the presence of strong, delayed negative feedback that is local in space. Such inhibitory feedback suppresses activity which develops in a localized region. The excitatory feedback, in turn, induces activity growth in nearby unadapted locations, thereby causing the propagation of the profile. We first present a simple way of incorporating adaptation in the population rate dynamics, and then study its effect on the network spatiotemporal state.

We incorporate adaptation by the following model:

$$\tau_0 \frac{d}{dt} m(\theta, t) = -m(\theta) + [I(\theta, t) - I_a(\theta, t) - T]_+, \tag{13.75}$$

where the total input $I(\theta, t)$ is given by eq. 13.12, and where the adaptation current $I_a(\theta, t)$ obeys a linear dynamical equation:

$$\tau_a \frac{dI_a(\theta, t)}{dt} = -I_a(\theta, t) + J_a m(\theta, t). \tag{13.76}$$

The parameter $J_a > 0$ measures the strength of the adaptation and τ_a is its time constant, which will be assumed to be large compared to τ_0. Note that the adaptation can be thought of as a slow local negative feedback, which we take to be linear.

In the absence of interaction between the neurons, and with a suprathreshold stimulus ($C > 1$) constant in time, the fixed point of the dynamics is given by

$$m(\theta) = G(C - T) \tag{13.77}$$

$$I_a(\theta) = J_a m(\theta) \tag{13.78}$$

where the single-neuron gain G is given by

$$G = \frac{1}{1 + J_a}. \tag{13.79}$$

This fixed point is always stable. Thus, for an isolated neuron, the slow adaptation current does not generate persistent oscillation, and the only effect of the adaptation at the fixed point is simply to reduce the gain of the neuron by a factor $1 + J_a$. A reasonable value for the adaptation strength is $J_a = 1$. With this strength, the firing rates at large time are reduced by 50% compared to the situation without adaptation. This is compatible with experimental data concerning spikes adaptation of cortical neurons (Connors, Gutnick, Prince 1982; Ahmed, Anderson, et al. 1994).

The stationary solution of the network dynamic equations remains essentially the same as without adaptation. Here again, the only effect of the adaptation is to reduce the gain by the factor $1 + J_a$: the new fixed solution for $m(\theta)$ is as given above except that the parameters J_0, J_2, C, and T have to be divided by the factor $1 + J_a$. However, the presence of adaptation strongly affects the *stability* of this fixed-point solution, particularly when the spatial inhomogeneity of the stimulus is weak. For sufficiently strong adaptation, the fixed-point solution is unstable; instead, a new spatiotemporal solution appears as the system's attractor.

We first discuss the case of a homogeneous stimulus, $\Upsilon = 0$. The results of the stability analysis of the fixed point as a function of the interaction modulation and adaptation strength are summarized on the phase diagram of figure 13.11. The weak adaptation regime is marked by

$$J_a < \frac{\tau_0}{\tau_a}. \tag{13.80}$$

In this regime, the system's behavior is similar to that with no adaptation. When the

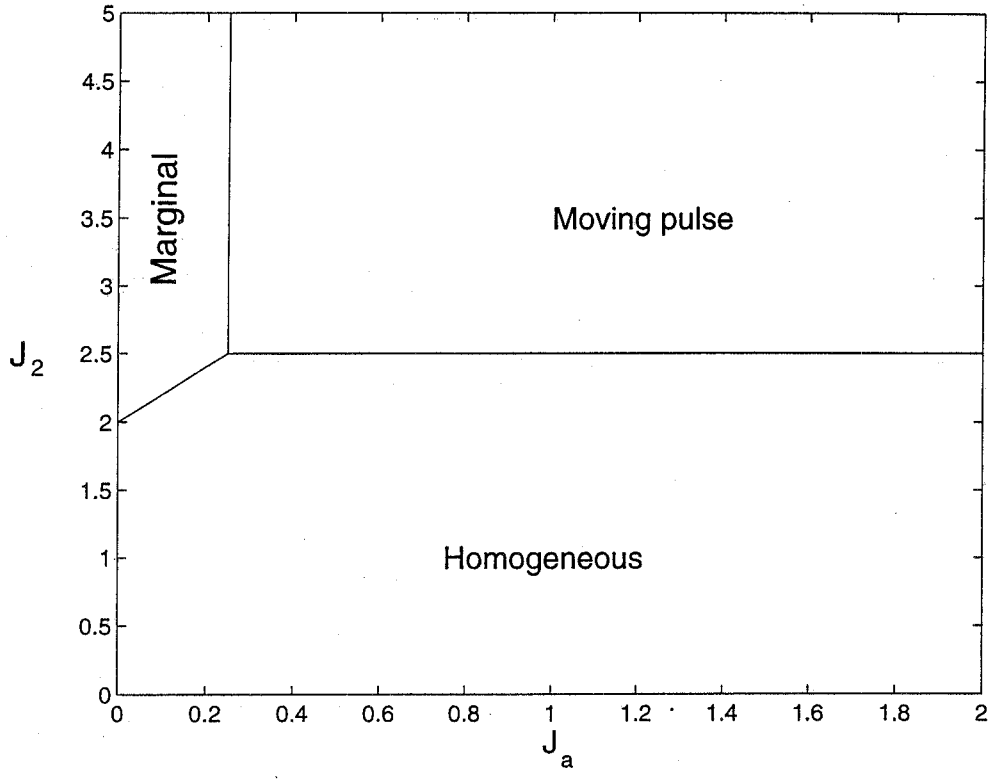

Figure 13.11
Phase diagram of the one-population rate model with firing adaptation, $\tau_a = 4\tau_0$.

modulation of the interaction J_2 is sufficiently small, the homogeneous state is stable. For a homogeneous input and $J_2 > 2(1 + J_a)$, the homogeneous state is unstable and a line of stationary attractors appears. As before, they correspond to stationary modulated activity profiles whose peaks are located at arbitrary positions. The shape of each activity profile can be deduced from the results of section 13.4 by normalizing the interactions J_0 and J_2 and the effective gain G by the factor $1/(1 + J_a)$.

In the strong adaptation regime

$$J_a > \frac{\tau_0}{\tau_a}, \tag{13.81}$$

the stationary homogeneous state is stable for $J_2 < 2(1 + \tau_0/\tau_a)$. Above this value, the state is destabilized in favor of a profile of activity that travels across the network (figure 13.12). The direction of the pulse movement depends on the initial conditions.

For $J_2 > 2(1 + \tau_0/\tau_a)$, the transition to a moving state as J_a increases above the value τ_0/τ_a (vertical line in figure 13.11) indicates the destabilization of the stationary

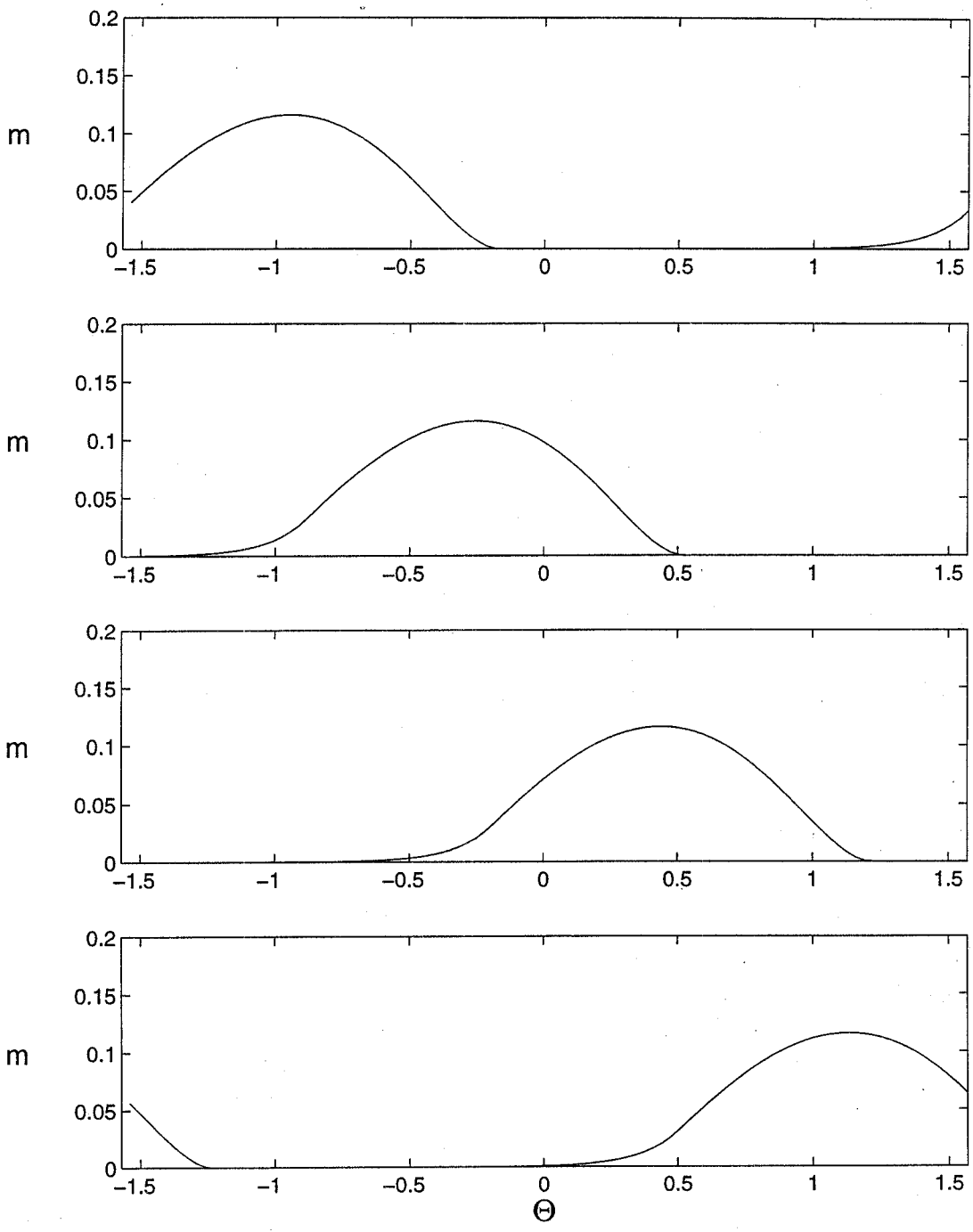

Figure 13.12
Traveling pulse of activity in the one-population rate model with adaptation. Parameters: $\tau_a = 4\tau_0$, $J_a = 1$, $J_0 = -2$, $J_2 = 6$, $C = 1.1$. Frames are for times $t = 0$, $5\tau_0$, $10\tau_0$, $15\tau_0$. Velocity of the pulse: $V = 0.1389\,\mathrm{rad}/\tau_0$.

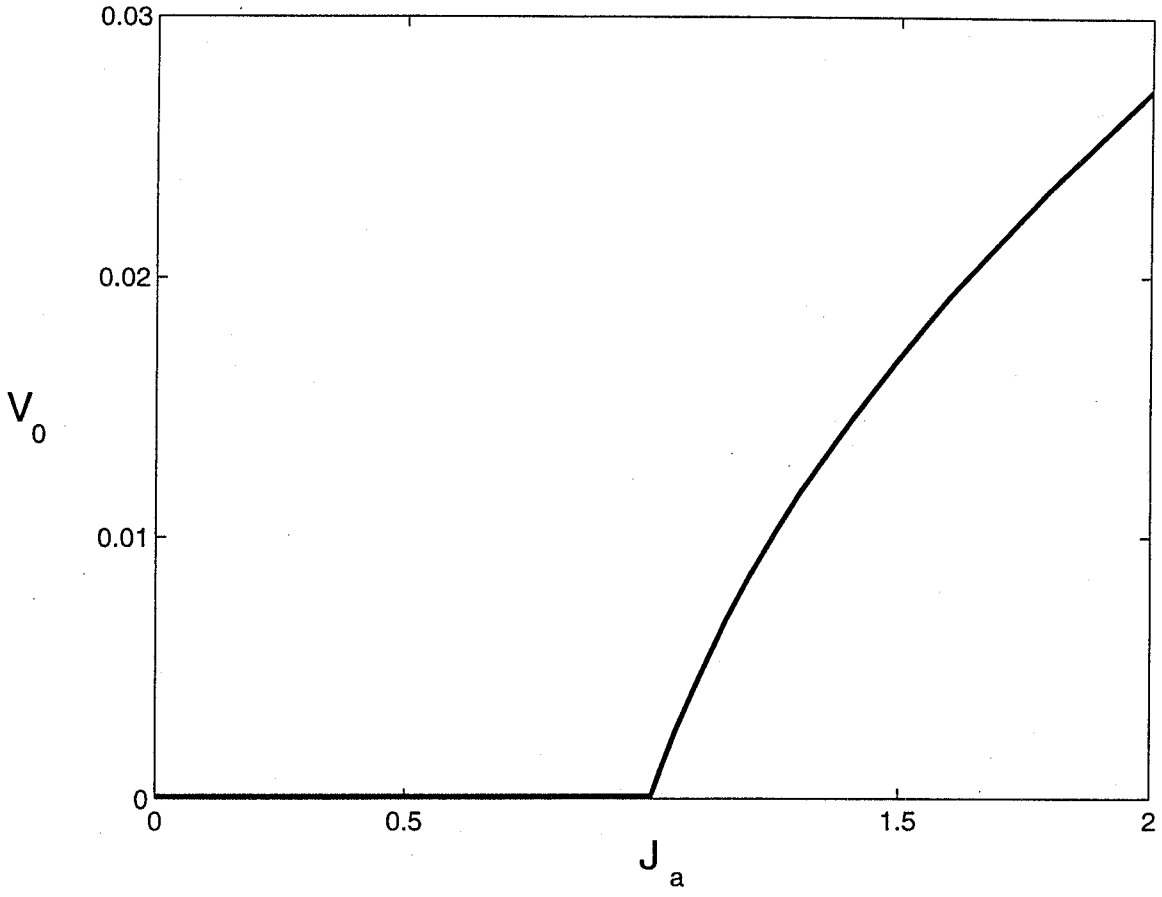

Figure 13.13
Velocity of the traveling pulse in the one-population rate model with adaptation against the adaptation strength J_a. Parameters: $\tau_a = 10\tau_0$, $J_0 = -2$, $J_2 = 6$, $C = 1.1$. Velocity in radians/τ_0.

inhomogeneous state is due to the appearance of an unstable transversal mode, which corresponds to the translation of the profile of activity across the network. Thus, on the right of the vertical line of figure 13.11, the network settles into a state where the activity profile moves without changing its shape. The velocity of the profile vanishes on the line as $J_a - \tau_0/\tau_a$. When J_a increases beyond this line, the velocity grows monotonically with J_a, as shown in figure 13.13.

For $J_a > \tau_0/\tau_a$, the destabilization of the stationary state as J_2 increases above $2(1 + \tau_0/\tau_a)$ (horizontal line in figure 13.11) corresponds to a pair of complex conjugate eigenvalues, whose real part becomes positive. This instability corresponds to a direct transition between the stationary homogeneous state and the traveling pulse. On this line, the half-width of the activity profile is $\pi/2$ and the velocity of the profile is

$$V_0 = \frac{1}{2\tau_a}\sqrt{J_a\frac{\tau_a}{\tau_0} - 1}. \tag{13.82}$$

The velocity is finite on the line except at $J_a = \tau_0/\tau_a$, where it vanishes.

When the stimulus is tuned, that is, $\varepsilon > 0$, three regimes exist depending on the value of ε. For ε sufficiently small ($\varepsilon < \varepsilon_1$), the hill of activity travels across the whole system but the velocity of the movement depends on the position of the hill. In particular, when the hill peak approaches the vicinity of the orientation of the stimulus, it is accelerated. For sufficiently large ε ($\varepsilon > \varepsilon_2$), one expects that the hill of activity will be pinned, with the maximum of activity located at the orientation of the stimulus. Finally, for $\varepsilon_1 < \varepsilon < \varepsilon_2$, the activity hill performs localized oscillations around the orientation of the stimulus. Figure 13.14 displays the behavior of the system in the three regimes.

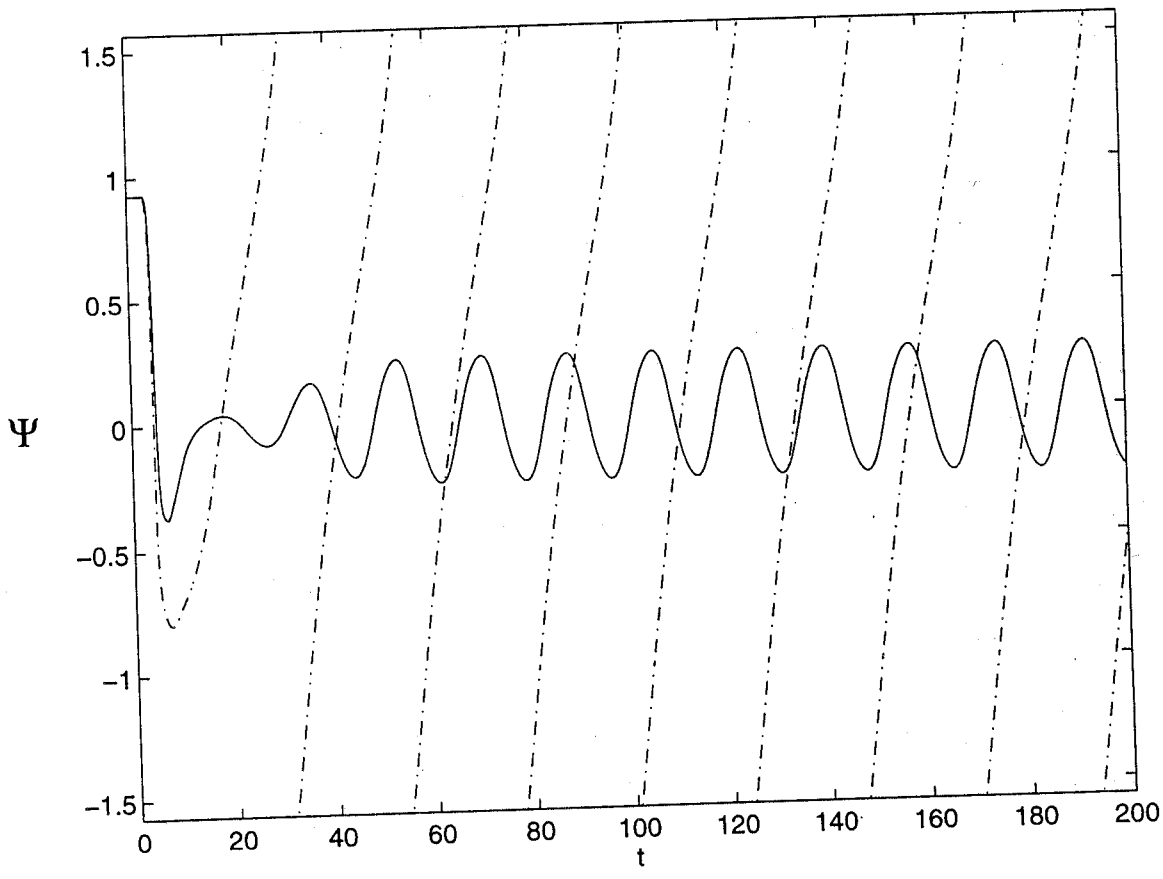

Figure 13.14
Pinning of the traveling pulse by the inhomogeneity of a tuned stimulus. Solid line: $\varepsilon = 0.2$; dash-dotted line: $\varepsilon = 0.06$. Same parameters as in figure 13.12.

13.6 Model with Short-Range Excitation

Until now, we have assumed a network architecture with space-dependent interactions whose range extended throughout the whole network (see eqs. 13.2 and 13.13). In this case, the strength of the spatial modulation of the cortical interactions is measured by the *amplitude* of their spatial modulation, for example, the parameter J_2 in eq. 13.13. In general, we expect that the range of the spatial modulation will also have an important effect on the spatial pattern of network activity. To study this issue, we consider in this section the case where the excitatory interactions decay exponentially with the distance between the interacting neurons. We will assume that the inhibitory interactions have significantly longer range than the excitatory interactions; hence we will approximate them by a global inhibition.

The exponential falloff of the excitatory interactions assumed here violates the periodic boundary conditions assumed until now. Periodic boundary conditions are appropriate for a network that processes angle variables such as orientation of an edge in the case of visual cortex, or representation of the direction of arm reaching movement in the case of motor cortex. For other features, such as tuning for spatial frequency in visual cortex or coding of place in hippocampus, such boundary conditions are not natural. Thus the present model will also illustrate to what extent the results we have obtained so far are sensitive to the idealized assumption about periodic boundary conditions and perfect translational symmetry.

Our model is a one-dimensional array of N neurons that code for a one-dimensional feature variable θ. The neurons are labeled by their PF, which is distributed uniformly in a range of size $2L$, that is, $-L < \theta < L$. The network dynamics are similar to those of the one-population rate model (eq. 13.11), with

$$I(\theta, t) = \sum_{\theta} J(\theta, \theta') m(\theta', t) + I^0(\theta - \theta_0). \tag{13.83}$$

The interaction between two neurons located at positions θ and θ' is of the form $J(\theta, \theta') = J(\theta - \theta')/N$, where

$$J(\theta - \theta') = \frac{2L}{\lambda}(-J_I + J_E \exp(-|\theta - \theta'|/\lambda)), \quad |\theta|, |\theta'| < L. \tag{13.84}$$

The parameter $J_I > 0$ represents a global inhibition. The second term with $J_E > 0$ is an exponentially decreasing excitation. The parameter J_E represents the amplitude of the spatial modulation of the cortical excitatory interactions, while the parameter λ denotes their spatial range. The external input has the form

$$I^0(\theta) = C(1 - 2\varepsilon + 2\varepsilon \exp(-|\theta|/\mu)). \tag{13.85}$$

The spatial dependence of the input is characterized by two parameters, namely, ε and μ. As in the case of the model investigated in section 13.3, ε is the amplitude of the spatial modulation of the input, generally defined as

$$\varepsilon = \frac{I^0_{max} - I^0_{min}}{2I^0_{max}}, \tag{13.86}$$

where $I^0_{max} = C$ is the maximum value of the external input and I^0_{min} is its minimum value. The parameter μ is the width of the input, which in the present model will be a free parameter.

We will assume that both λ and μ are on the scale of L but may be smaller than L. Thus, although the excitatory interactions are of a limited spatial range, each neuron (except at the boundaries) receives excitatory inputs from a sizable fraction λ/L of the N neurons. Thus, for large N, a continuum mean field description of the network dynamics is valid, yielding for the total input current at time t

$$I(\theta, t) = \int_{-L}^{+L} d\theta' J(\theta - \theta')m(\theta', t) + I^0(\theta - \theta_0). \tag{13.87}$$

The fixed-point state of the network is given by the following self-consistent equations:

$$m(\theta) = \left[\frac{-J_I}{\lambda} r_0 + \frac{J_E}{\lambda}\int_{-L}^{+L} d\theta' \exp(-|\theta - \theta'|/\lambda)m(\theta') + I^0(\theta - \theta_0) - T\right]_+, \tag{13.88}$$

where

$$r_0 = \int_{-L}^{+L} d\theta\, m(\theta). \tag{13.89}$$

Comparing eq. 13.88 with eqs. 13.16, 13.17, and 13.20, it is seen that the present model is more complex than our previous model. Because of the form of the present interaction function, the fixed-point equations cannot be reduced to a small number of global order parameters. Yet both models share the simplicity that within the *active* population the underlying equations are linear. In fact, differentiating eq. 13.88 twice with respect to θ in the regime where $m(\theta)$ is nonzero, we find that in this regime the activity profile obeys the following second-order linear differential equation:

$$\frac{d^2m}{d\theta^2} + \frac{m}{\Lambda^2} = \frac{d^2I^0}{d\theta^2} + \frac{1}{\lambda^2}\left(T + \frac{J_I}{\lambda} r_0 - I^0(\theta)\right), \tag{13.90}$$

where

$$\Lambda^2 = \frac{\lambda^2}{2J_E - 1}. \tag{13.91}$$

The above equation is supplemented with the following boundary conditions:

$$m(0) = -\frac{J_I r_0}{\lambda} + C - T + \frac{J_E}{\lambda}\int_{-L}^{L} \exp(-|\theta|/\lambda) m(\theta)\, d\theta \tag{13.92}$$

and

$$\frac{dm(0^{\pm})}{d\theta} = \frac{dI^0(0^{\pm})}{d\theta}. \tag{13.93}$$

Finally, r_0 has to be calculated self-consistently, using eq. 13.89. Eqs. 13.89–13.93 can be solved for broad and narrow profiles for the stimulus of the form given by eq. 13.85. We first consider the case of a homogeneous input, $\varepsilon = 0$.

13.6.1 Broad Activity Profile

The simplest solution to eqs. 13.91–13.94, for $I^0(\theta) = C$, that is, $d^2 I_0/d\theta^2 = 0$, is obtained assuming that the local fields on all the neurons are above threshold. The solution is of the form

$$m(\theta) = \begin{cases} (C - T)(A - B\cosh(\theta/\Lambda)) & J_E < \frac{1}{2} \\ (C - T)(A\cos(\theta/\Lambda) - B) & J_E > \frac{1}{2}. \end{cases} \tag{13.94}$$

The constants $A > B > 0$, determined by the boundary conditions and eq. 13.90, depend on the parameters J_I, J_E, L, and λ, as detailed in Hansel and Sompolinsky 1997. An example of the activity profile in this regime can be seen in figure 13.15, where the linear solution is unique and centered at $\theta = 0$. Contrary to the previous case, where the linear solution for homogeneous external inputs was uniform, here the corresponding solution is not uniform. The θ dependence of this solution is due to boundary effect: neurons close the boundaries receive less excitatory feedback; hence their level of activity is decreased.

13.6.2 Narrow Profiles and Marginal Phase

The above broad solution is valid, provided the $m(\theta)$ of eq. 13.94 is positive and does not vanish in the range $-L < \theta < +L$. Whether this condition holds depends on both J_E and λ. For $J_E < 1/2$, the broad solution is indeed a valid solution for all λ. For $J_E > 1/2$, however, the above solution is positive for all θ only for sufficiently

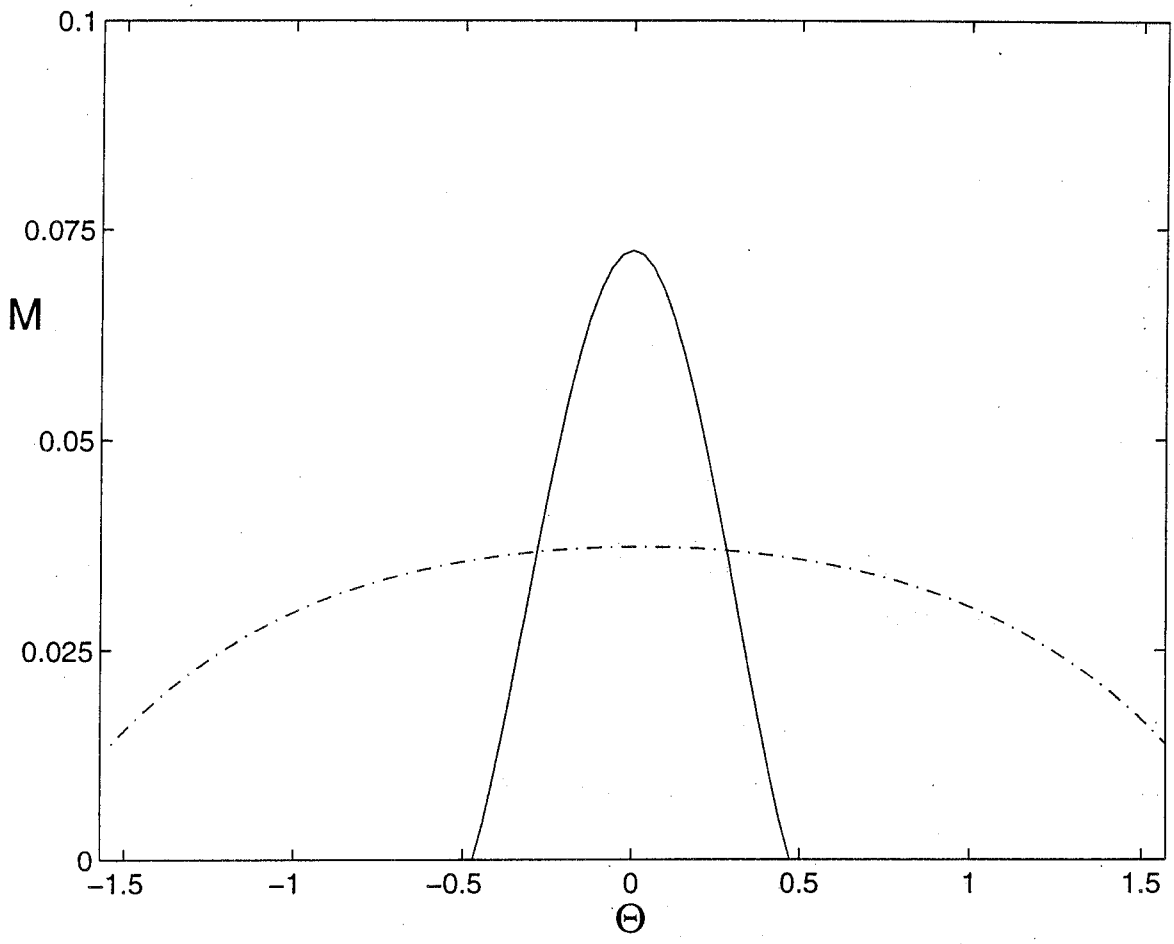

Figure 13.15
Profile of activity in the one-population rate model with short range excitation and open boundary conditions for $L = \pi, J_0 = -0.2, \lambda = 0.2, C = 1.01$. Dash-dotted line: broad profile for $J_2 = 0.45$; solid line: narrow profile for $J_2 = 1$.

large λ/L. If $\lambda < \lambda_c$, the above solution becomes negative, hence not valid. Instead, a solution with a narrow profile appears in which only part of the population is active. This solution is not unique. Because the active population does not receive inputs from neurons near the boundary, the activity of the neurons does not depend on their location relative to the boundary unless the activity profile is close to the boundary. Thus the narrow solution of eq. 13.90 (again, with $I^0(\theta) = C$) is of the form

$$m(\theta) = M(\theta - \Psi), \quad -L + \theta_C < \Psi < L - \theta_C, \tag{13.95}$$

where

$$M(\theta) = (C - T)A[\cos(\theta/\Lambda) - \cos(\theta_c/\Lambda]_+. \tag{13.96}$$

The width of the profile is given by

$$\theta_C(J_E) = \Lambda(\pi - \arctan\sqrt{2J_E - 1}). \tag{13.97}$$

The constant A is related to the gain G through eq. 13.24. It can be shown that the gain of the narrow profile is

$$G = \frac{1 - \cos(\theta_C/\Lambda)}{f(\theta_C)(J_I - J_C)}, \tag{13.98}$$

where

$$f(\theta_C) = \left(\frac{\theta_C}{\lambda} + 1\right) 2\cos\left(\frac{\theta_c}{\Lambda}\right) \tag{13.99}$$

and

$$J_C = \frac{tan^2\left(\frac{\theta_c}{\Lambda}\right)}{2\left(\frac{\theta_C}{\lambda} + 1\right).} \tag{13.100}$$

Note the similarity between these equations and those of the marginal state in the periodic long-range model of section 13.4 (eqs. 13.55–13.57). The critical value of λ (or J_E) for which this phase exists is given by the condition that θ_C approaches the boundary, namely,

$$\theta_C = L \tag{13.101}$$

If L is large compared to the range of interactions λ, this marginal phase therefore exists for all λ as long as $J_E > 1/2$ (see figure 13.15). The phase diagram of the model is shown in figure 13.16. It should be noted that the shape of the activity profile is determined only by the modulated component of the interactions. However, as in the periodic system, the stability of all the above solutions depends also on the value of J_I.

In conclusion, the above results demonstrate the respective roles of the amplitude and the range of the cortical feedback excitation. The phase diagram (figure 13.16) shows that when the range of the excitatory interactions is small compared to the total extent of the network, namely, $\lambda \ll L$, the onset of the marginal phase and the associated emergence of narrow activity profiles in response to broadly tuned input depend on the amplitude of the spatial modulation of the cortical interactions and are insensitive to its range. On the other hand, the *width* of the narrow activity profile depends on both λ and J_E, as seen from eqs. 13.91 and 13.97.

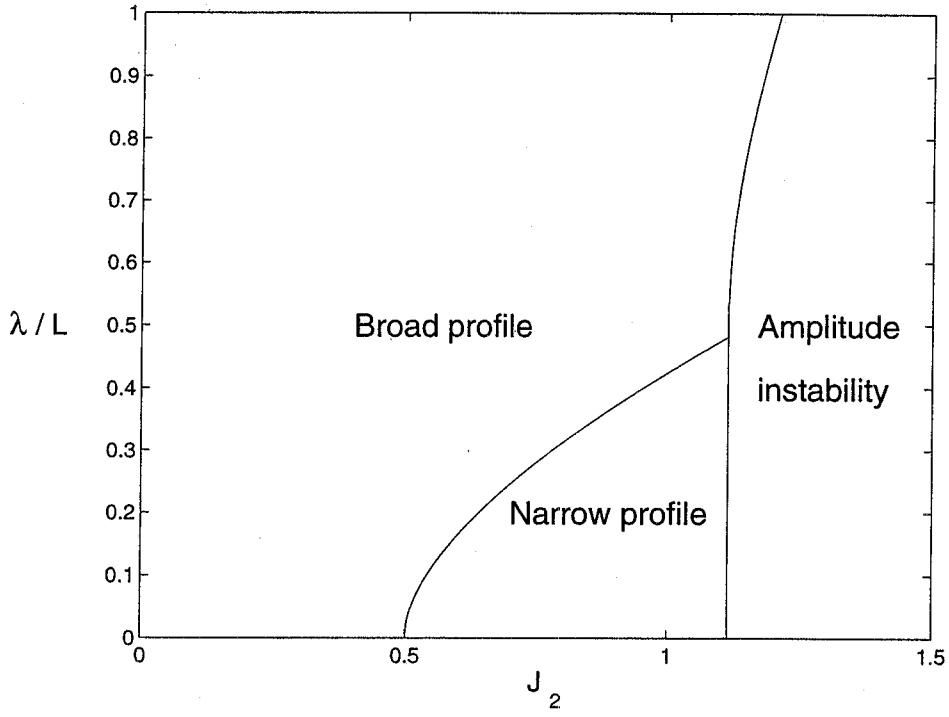

Figure 13.16
Phase diagram of the one-population rate model with short range excitation and open boundary conditions for $J_0 = -0.2$. The stimulus is homogeneous.

13.6.3 Tuned Input

Considering next the case of an input of the form of eq. 13.85, with $\varepsilon > 0$, we focus on the dependence of the resultant activity profile on the parameters C, ε, and μ of the external input. It is easy to see from the fixed-point equation that the profile of activity depends on C and ε through the *effective stimulus tuning* Υ defined by eq. 13.31. In particular, in the absence of cortical interactions, the resultant activity profile is the same as that of the input except for the thresholding effect. Thus, for strongly tuned input, defined by

$$\Upsilon > \tfrac{1}{2}, \tag{13.102}$$

the solution of eq. 13.88 has a narrow activity profile, with

$$m(\theta) \propto [\exp(-|\theta - \theta_0|/\mu) - \exp(-|\theta_C - \theta_0|/\mu)]_+, \quad \Upsilon > 1/2,\ J_I = J_E = 0, \tag{13.103}$$

where

$$\theta_C = -\mu \ln\left(1 - \frac{1}{2\Upsilon}\right). \tag{13.104}$$

This function is depicted in figure 13.17 for $\mu = 0.05$ and $\mu = 1.5$. When the stimulus tuning is weak, that is, $\Upsilon < 1/2$, the activity profile is broad, namely, all the neurons are above threshold.

We now consider the effect of the cortical excitation on the tuning of the network activity. We will focus on the parameter regime where the network possesses a marginal phase, namely,

$$J_E > 1/2, \quad J_I > J_C, \quad \lambda < \lambda_c. \tag{13.105}$$

As in our previous model the most important role of the tuned stimulus is to select from the continuum of fixed points (eq. 13.95) the profile

$$\Psi = \theta_0. \tag{13.106}$$

It can be shown that the general solution of the narrow profile in eq. 13.91 is of the form

$$m(\theta) = (C - T)[A\cos(\theta/\Lambda) - \Upsilon B|\sin(\theta/\Lambda)| + \Upsilon D\exp(-|\theta|/\mu) + F]_+. \tag{13.107}$$

Thus, for small Υ, the form of the activity profile is close to that for a uniform input (eq. 13.96). Note that despite the exponential shape of the external stimulus, the dominant part of the network activity profile is in this case of a cosine form. The cosine form of the activity profile in the marginal phase, predicted by eq. 13.36, is therefore not special to interactions with the cosine form such as eq. 13.13. Instead, the cosine form for the profile is quite general and is related to the fact that the instability to the formation of these patterns occurs first at long wavelength modes.

Recall that in the model of section 13.4, where both the excitatory interactions and the stimulus had long spatial range, the width of the activity profile was determined, in the marginal phase, by the cortical interactions and was rather insensitive to the effective stimulus tuning Υ. In the present model, however, the tuning of the network activity is in general a complicated function of both Υ and μ through the values of the constants A, B, D, and F (Hansel and Sompolinsky 1997). The qualitative behavior of the tuning width can be understood by considering narrow stimulus and broad stimulus limits.

Narrow Stimulus This case is defined as $\mu/\lambda \ll 1$, where the behavior depends on the effective stimulus tuning Υ.

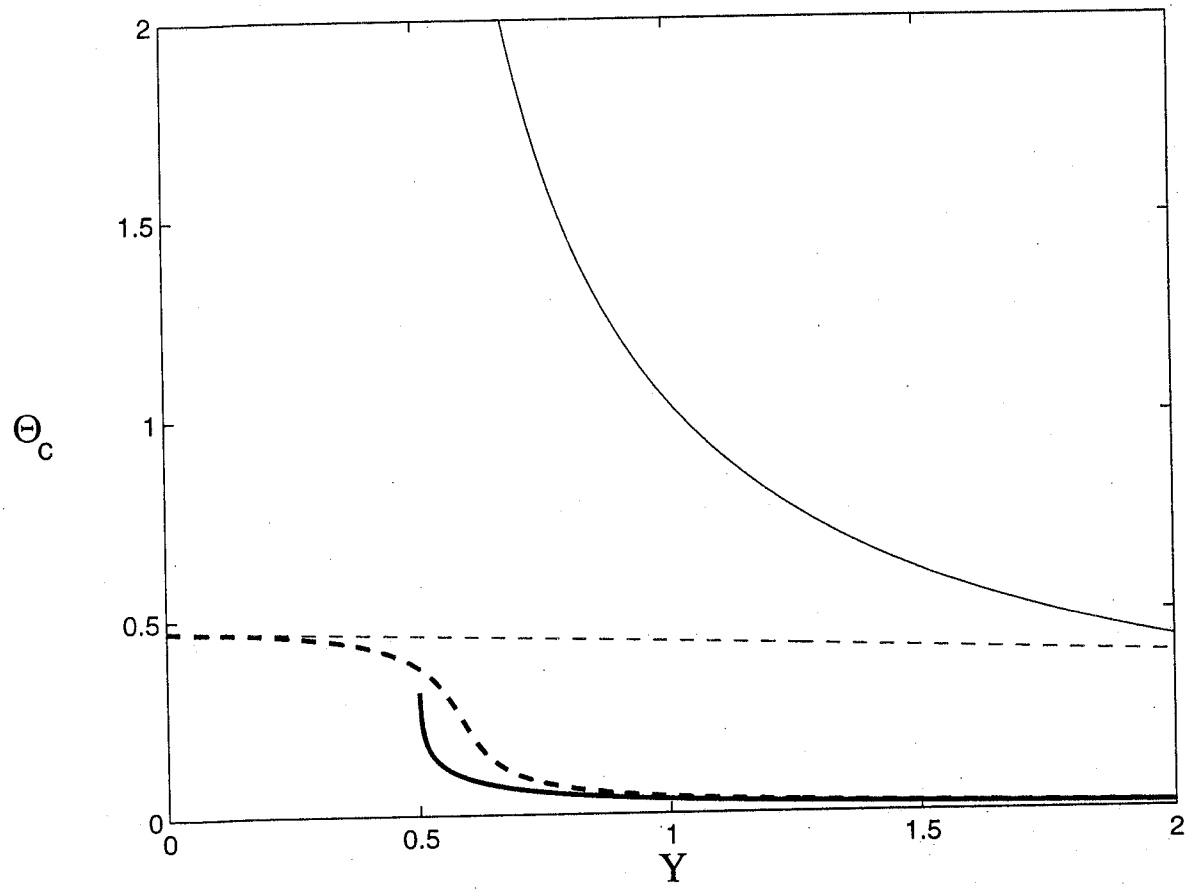

Figure 13.17
Width θ_c of the activity profile in the rate model with short range excitation and open boundary conditions; θ_c is plotted as a function of Υ. For $\mu = 1.5$, thin solid line: afferent mechanism; thin dashed line: marginal phase. For $\mu = 0.05$, thick solid line: afferent mechanism; thick dashed line: marginal phase. Parameters: $\lambda = 0.2, J_0 = -0.2, J_2 = 1$ for the marginal phase, and $J_0 = 0$; $J_2 = 0$ for the afferent mechanism.

STRONGLY TUNED INPUT In the case $\Upsilon > 1/2$, we find that the width of the profile is

$$\theta_C \simeq -\mu \ln\left(1 - \frac{1}{2\Upsilon}\right), \quad \mu/\lambda \ll 1. \tag{13.108}$$

Thus the width of the tuning is the same as if there were no cortical interactions; namely, it is determined by the width of the input. This is expected because in this regime the tuning provided by the external input (of the order μ) is much sharper than that provided by the interactions (of the order λ).

WEAKLY TUNED INPUT If $\Upsilon < 1/2$, we find that the tuning of the neuronal response is independent of the tuning of the input and is given by eq. 13.97. Therefore, in this limit, the shape of the activity profile is determined essentially by the cortical interactions; the main effect of inhomogeneity in the external input is to select among the continuum of possible states that state in which the peak in the activity matches the stimulus feature, namely, $\Psi = \theta_0$. The crossover between the two regimes occurs in the region $\Upsilon \simeq 1/2$. The size of the crossover region is a decreasing function of μ/λ.

Broad Stimulus In the limit $\mu/\lambda \gg 1$, which corresponds to an input much broader than the excitatory interaction, the tuning of the input does not much affect the shape of the tuning curve; as in the previous case, its main effect is to select the state with $\Psi = \theta_0$. An exception is the case of a stimulus with intensity near threshold, namely, $\Upsilon \gg 1$: once the single-neuron thresholding effect becomes dominant, it sharpens the tuning curve beyond the sharpening provided by the cortical mechanisms.

Figure 13.17 shows θ_C for various stimulus parameters obtained by a full solution of the model with tuned input. In the case of μ/λ large, θ_C is determined by the cortical interactions, and Υ does not significantly affect it. On the other hand, when μ/λ is small, there is a pronounced decrease of θ_C when $\Upsilon \geq 1/2$, which agrees with the analysis above. Comparing these results with those of figure 13.5 (section 13.4), we see that figure 13.17 is similar to the cases $\mu/\lambda > 1$. The effect of the width of the stimulus is most pronounced in the regime of small μ/λ. Here, increasing Υ causes a sharp crossover from interaction-dominated tuning ($\Upsilon < 1/2$) to afferent-dominated tuning ($\Upsilon > 1/2$).

13.6.4 Intrinsic Moving Profiles

We now turn briefly to moving profiles with homogeneous external input. The addition of adaptation current to the present model, as in eqs. 13.75 and 13.76, tends to destabilize the stationary profile of the marginal phase and to induce moving

activity profiles similar to those of the periodic system (as shown in "Instability of the Marginal Phase Due to Adaptation" in chapter appendix B). Although the boundaries do not affect the existence of stationary narrow solutions in the networks's interior, the situation is different in the case of moving solutions. The reason is that in the moving state all the neurons are active, hence they do feel the influence of the boundaries. The effect of the boundaries on the wave propagation depends on the amplitude of the adaptation current. For relatively low values of J_a (but sufficient to generate moving profiles), the boundaries act as reflecting walls. The profiles bounce between the two boundaries, as shown in figure 13.18A. On the other hand, for strong adaptation, the boundaries act as sinks; once the symmetry of the direction of movement is broken by the initial conditions, the profiles keep moving in the same direction, across the network, as shown in figure 13.18B. It is interesting to note that the boundaries act here like an inhomogenous external input peaked at the center in the periodic architecture, as in section 13.5.2; they distort the motion of the profile but do not reverse its direction of motion. On the other hand, in the case of relatively low adaptation, the boundaries act as relatively strong inhomogeneities that localize the moving profile, as shown figure 13.12.

13.7 Network Model with Conductance-Based Dynamics

13.7.1 Conductance-Based Dynamics of Point Neurons

This section describes a dynamic model based on the well-known Hodgkin and Huxley–type equations (see chapter 10, this volume) for a single space-clamped neuron and synaptic conductances opened after the occurance of action potential in the presynaptic neurons. The equation satisfied by the membrane potential of neuron θ of type α is

$$\frac{d}{dt}V^{\alpha}(\theta, t) = -G^{\alpha}_{leak}(V^{\alpha}(\theta, t) - V_{leak}) - I^{\alpha}_{gated}(\theta, t) + I^{\alpha}(\theta, t). \tag{13.109}$$

For simplicity, we assume the membranes' capacitance is 1. The first term on the right-hand side of eq. 13.109 corresponds to the contribution of the leak current, which has voltage-independent conductance G^{α}_{leak}. The current I^{α}_{gated} represents the voltage-gated ionic currents, which are in particular responsible for the generation of action potential. The last term of eq. 13.109 incorporates all the synaptic inputs converging on the neurons and consists of the three components described in eq. 13.1. Each of these components represents synaptic conductances,

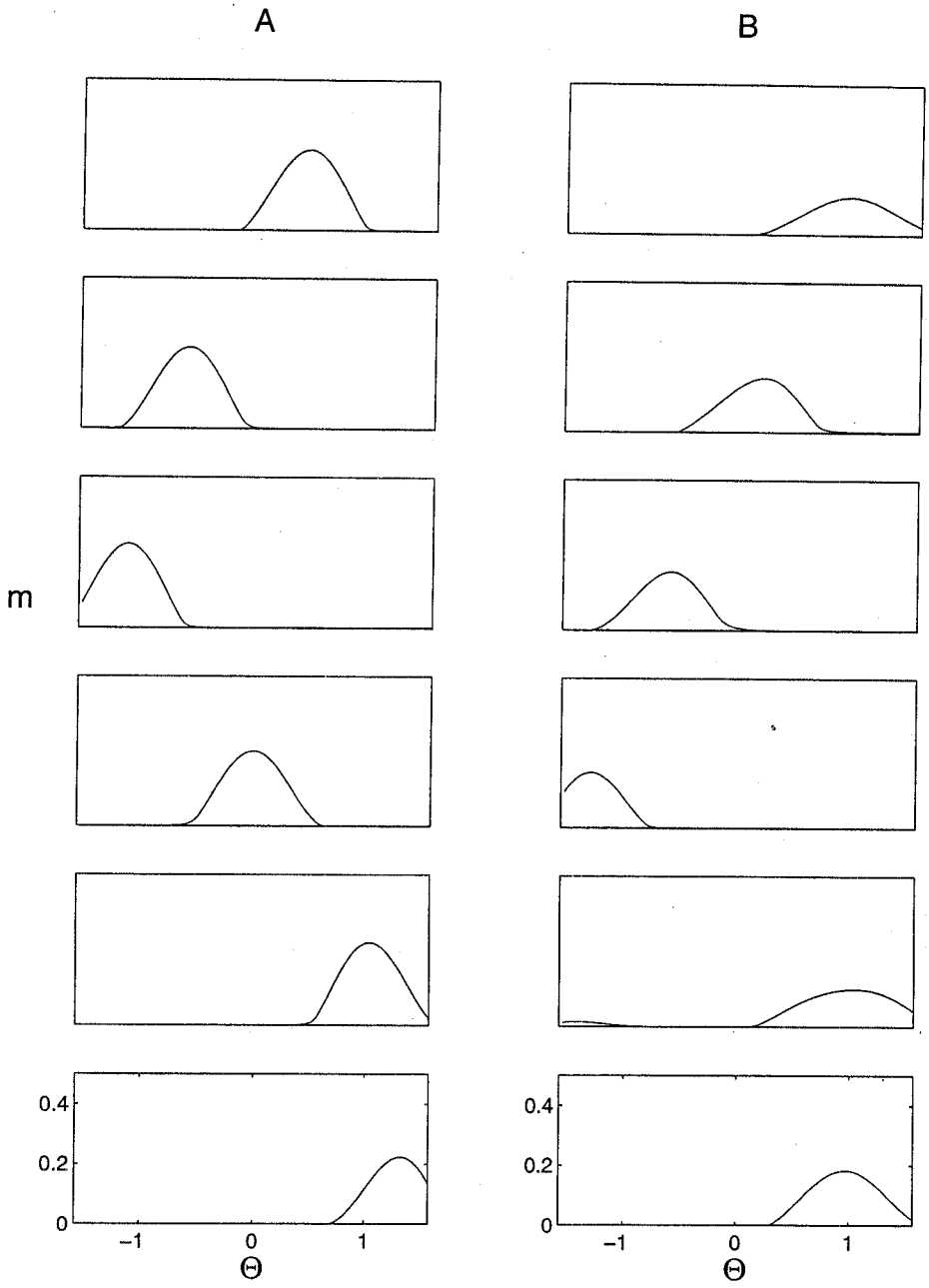

Figure 13.18
Traveling pulse in the short range model with open boundary conditions and adaptation. Parameters: $L = \pi, J_0 = -0.2, J_2 = 1, \lambda = 0.2, C = 1.1, \tau_a = 10\tau_0$. (A) $J_a = 0.5$. The pulse is oscillating between the boundaries. Times (top to bottom; in units of τ_0): $t = 0$, 20, 30, 60, 80, 90. (B) $J_a = 1$. The pulse is always moving in the same direction. Times (top to bottom; in units of τ_0): $t = 0$, 5, 15, 25, 30, 35.

$$I^{\alpha\beta}(\theta, t) = g^{\alpha\beta}(\theta, t)(V^{\beta} - V^{\alpha}(\theta, t)), \tag{13.110}$$

triggered by the action potentials of the presynaptic neurons,

$$g^{\alpha\beta}(\theta, t) = \frac{1}{N_\beta}\sum_{i=1}^{N_\beta} g^{\alpha\beta}(\theta - \theta_i)\sum_{t_i} f^{\beta}(t - t_i), \quad \beta = E, I \tag{13.111}$$

$$g^{\alpha 0}(\theta, t) = \frac{1}{N_0}\sum_{i=1}^{N_0} g^{\alpha 0}(\theta, i)\sum_{t_i} f^{0}(t - t_i). \tag{13.112}$$

The synaptic time course is described by the synaptic response function $f^{\beta}(t - t_i)$, where t_i is the occurrence time for a spike in neuron i (of type β). A frequently used form is

$$f(t) = A(e^{-t/\tau_1} - e^{-t/\tau_2}), \quad t \geq 0, \tag{13.113}$$

and $f(t) = 0$ otherwise. The normalization constant A is such that the peak value of f is 1. The characteristic times τ_1 and τ_2 are, respectively, the synaptic rise and decay times, whose value may be different for the different types of synapses. The synaptic reversal potentials are denoted V_α.

The functions $(1/N_\beta)g^{\alpha\beta}(\theta - \theta')$ represent the peak value of the synaptic conductances between a presynaptic neuron, $\beta\theta'$, and a postsynaptic one, $\alpha\theta'$. These functions are proportional to the interaction functions $J^{\alpha,\beta}(\theta - \theta')$ introduced above. The spatial organization of the input from the stimulus is encoded in $g^{\alpha 0}(\theta, i)$. Because we are not modeling the architecture and dynamics of the input network in detail, we will assume the incoming spikes to a neuron obey Poisson statistics at rates that give rise to a fluctuating input conductance with a time average of the form

$$\langle g^{\alpha 0}(\theta, t)\rangle_{av} = g^{\alpha 0}(\theta - \theta_0), \tag{13.114}$$

where θ_0 is the stimulus feature. For instance, the function $g^{\alpha 0}(\theta - \theta_0)$ may be proportional to $I^{\alpha 0}(\theta - \theta_0)$ in eq. 13.3.

13.7.2 Mean Field Theory of Asynchronous States

In general, the network described above may develop complex dynamical behaviors that are hard to analyze. A particularly simple case is when the network settles in an asynchronous state, which may occur if the external input is statistically stationary and the temporal fluctuations of the inputs to different neurons are only weakly correlated. Under these conditions, if the network is large enough, it may settle into

a state where the correlations between the activities of different neurons are weak, despite their interactions. In such a state, the total synaptic conductances on each neuron is constant in time, up to small fluctuations that vanish in the limit of a large network, $N_\alpha \to \infty$. Whether the network settles into a synchronous or asynchronous state depends on the network parameters (as described in detail in Hansel and Sompolinsky 1996).

In the asynchronous state, the feedback from the network on each neuron can be described in terms of constant currents and conductances, called "mean fields," which obey certain self-consistent equations. In our case, the total synaptic conductance from the α population on neuron θ is constant in time and is given by

$$g^{\alpha\beta}(\theta) = \int_{-\pi/2}^{+\pi/2} \frac{d\theta'}{\pi} J^{\alpha\beta}(\theta - \theta') m^{\beta}(\theta'), \quad \beta = E, I, \tag{13.115}$$

where $m^{\alpha}(\theta)$ is the time-average firing rate of neuron θ in the population α.

Taking into account the stationarity of the synaptic conductances, eq. 13.109 can be written as a single-neuron dynamic equation:

$$\frac{d}{dt} V^{\alpha}(\theta, t) = -(g^{\alpha}(\theta) + \delta g^{\alpha 0}(\theta, t)) V^{\alpha}(\theta, t) - I_{gated}(\theta, t) + I^{\alpha}(\theta), \tag{13.116}$$

with

$$g^{\alpha}(\theta) = G^{\alpha}_{leak} + g^{\alpha E}(\theta) + g^{\alpha I}(\theta) + g^{\alpha 0}(\theta - \theta_0) \tag{13.117}$$

$$I^{\alpha}(\theta) = (g^{\alpha E}(\theta) + g^{\alpha 0}(\theta - \theta_0)) V^{E} + g^{\alpha I}(\theta) V^{I}. \tag{13.118}$$

The term $\delta g^{\alpha 0}(\theta, t)$ represents the fluctuations in the input conductance due to the Poisson statistics of the incoming spikes. The currents I^{α} and conductances g^{α} themselves depend on the time-average activity profiles, $m^{\alpha}(\theta)$, of the neurons in the network through eq. 13.115. Thus to complete the solution, we have to calculate the time-average firing rates of single neurons obeying dynamics of the form of eq. 13.116. This results in self-consistent integral equations for the stationary activity profiles of the form $m^{\alpha}(\theta) = F(\theta, \{m^{\beta}(\theta')\})$. A similar approach can be used in principle to study the properties of the network in cases where the stimulus varies slowly with time.

In section we analyzed the network properties using simplified rate dynamics. Here we use numerical simulations to study the properties of a network with the same architecture as that of the rate model but with conductance-based dynamics. We first specify below the details of the model and then compare the numerical results with the theoretical prediction of the rate model.

13.7.3 Details of the Numerical Simulations

Single-Neuron Dynamics We have studied eq. 13.109 with voltage-gated current, I_{gated}, which incorporates sodium (I_{Na}) and potassium (I_K) currents, responsible for spike generation, as in the standard Hodgkin-Huxley model. It also includes a non-inactivating persistent sodium current, (I_{NaP}), and an A-current (I_A), known to be present in cortical and hippocampal cells (Llinás 1988; Stafstrom, Schwindt, and Crill 1982; Gustafsson et al. 1982; see also chapter 5, this volume). The first current enhances the excitability of the cells at voltages near threshold, leading to a frequency-current relationship that increases continuously from zero and thereby increases the dynamic range of the neurons. The A-current reduces the gain of the neurons, and thereby suppresses their maximal rate (Connor, Walter, and Mckown 1977; Rush and Rinzel 1994).

Below we will also study the effect of adaptation on the network state. Because regular spiking pyramidal cells in cortex display spike adaptation (Connors, Gutnick, and Prince 1982), but fast spiking neurons do not, we incorporate adaptation only in the excitatory population, which corresponds to the regular spiking pyramidal cells. This adaptation is introduced by adding to the single-neuron dynamics a slow potassium current with a relatively large time constant, chosen independently of the membrane potential for the sake of simplicity and in the range 10–100 msec in agreement with a recent study of firing adaptation (Ahmed, Anderson, et al. 1994).

The full kinetic equations of these currents are given in chapter appendix C, along with all the parameter values used in our simulations, which correspond to a cell with a resting potential, $V_{rest} = -71\,\text{mV}$, and a membrane time constant at rest, $\tau_0 = 10\,\text{msec}$. Typical values used below are $\tau = 60\,\text{msec}$ and $g_a = 10\,\text{mS/cm}^2$. As illustrated in figure 13.19, this corresponds to a reduction in the firing rate on the order of 50%, which agrees with the experimental results. Traces of the membrane potentials of single, isolated excitatory and inhibitory neurons are shown in figure 13.20.

Network Architecture We have simulated a network with an equal number of excitatory and inhibitory neurons; within each population, the neurons have identical intrinsic and synaptic properties. The synaptic inputs are modeled according to eqs. 13.109–13.113. For the spatial modulation of the synaptic conductances $g^{\alpha\beta}(\theta - \theta')$ in eq. 13.111, we take a square function. All pairs of excitatory neurons whose PFs differ by an amount smaller in absolute value than a given value, $\delta\theta$, are connected with the same connection strength; if the difference is larger than this cutoff, the connection between them is zero. In the present simulations, we use $\delta\theta = 30°$ as the

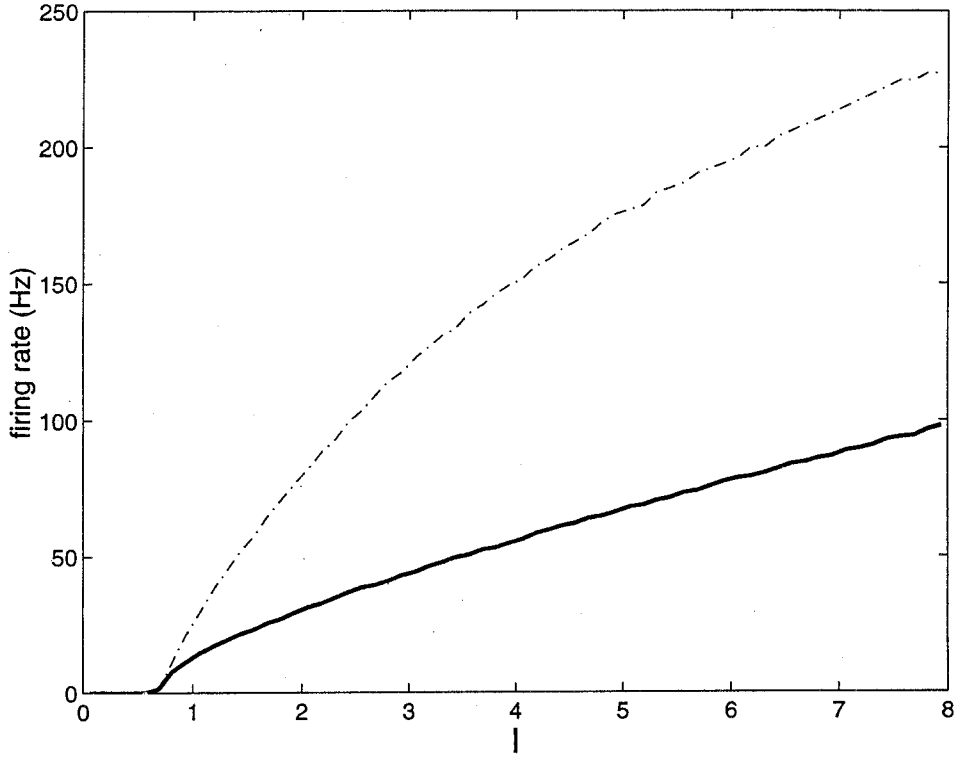

Figure 13.19
Firing rate of the neurons in the excitatory population in the spiking neuron network model (no interaction). Solid line: firing rate at large time upon injection of a constant current; dash-dotted line: instantaneous firing rate from the first interspike interval after the injection of the current. The adaptation time constant is $\tau_a = 60\,\text{msec}$. The adaptation maximal conductance is $g_a = 10\,\text{mS/cm}^2$.

range of the excitatory interactions. The inhibition to inhibitory neurons is assumed to be global and homogeneous; each inhibitory neuron is assumed to inhibit all the excitatory neurons with the same maximal synaptic conductance (although the maximal conductance of the inhibition to the inhibitory neurons can differ from that of the excitatory neurons). The synaptic action of the excitatory neurons on the inhibitor neurons is also assumed to be global. For simplicity, propagation delays are not included in the model. The values of the synaptic strengths and time constants are give in table 13.1 (chapter appendix C).

Equation 13.112 for the external stimulus is implemented by assuming

$$g^{\alpha 0}(\theta, t) = g^0 \sum_{t_0} f^0(t - t_0), \tag{13.119}$$

where t_0 is the arrival times of spikes generated by a Poisson process with a rate $C(1 - \varepsilon + \varepsilon\cos(2\theta - \theta_0))$. Here the stimulus intensity C is given in terms of the input

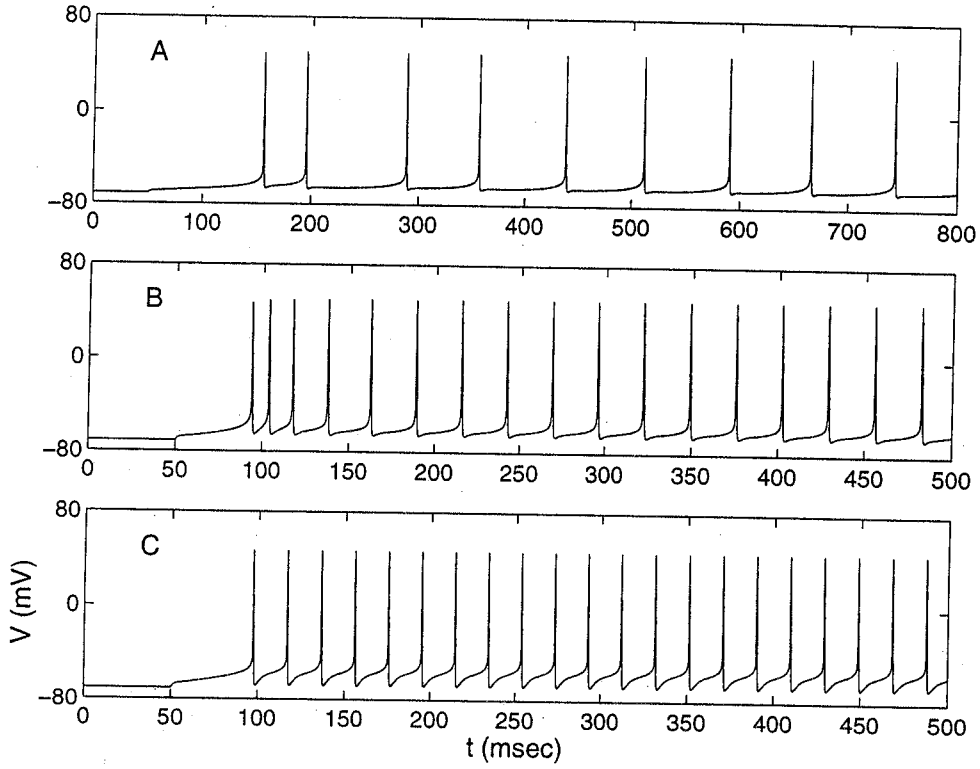

Figure 13.20
Membrane potential of the neurons in the spiking network model upon injection of a constant current I_0 (no interaction). (A) Excitatory neuron. Parameters are given in chapter appendix C. Adaptation parameters as in figure 13.19. $I_0 = 1\,\mu A/cm^2$. (B) Adaptation parameters as in panel A but with $I_0 = 2.5\,\mu A/cm^2$. (C) Inhibitory neuron. Parameters are given in table 13.1 (chapter appendix C). $I_0 = 2.5\,\mu A/cm^2$.

firing rate onto the maximally stimulated cortical neuron, which ranges between 400 Hz and 2,000 Hz. We assume that the characteristics of the afferent synapses are the same for all the neurons. The values of the strength g^0 and the time constant of the input conductance are given in table 13.1.

Below we present the results of the simulations with $N_E = N_I = 512$ neurons.

13.7.4 The Marginal Phase

Stationary Stimulus In section 13.4.4 (see "Homogeneous Input, Marginal Phase"), it is predicted that if the orientation-dependent component of the cortical interactions is strong enough compared to the inverse gain of single neurons, then the system will exhibit a marginal phase where even in the absence of orientation-specific input it will spontaneously form a spatially inhomogeneous activity profile. In this *marginal phase*, and in the presence of weakly tuned stimulus, the orientation tuning of the system is strongly enhanced by the cortical feedback interactions. There is a

range of parameters for which our model shows a similar enhancement of orientation tuning by the cortical feedback interactions. Indeed, we have found that for a sufficiently low value of g_a, a marginal phase appears (the results presented in this section were obtained for $g_a = 0\,\mathrm{mS/cm^2}$).

The network response to an homogeneous input ($C = 1{,}000\,\mathrm{Hz}$) is shown in figure 13.21A. The network settles spontaneously in an inhomogeneous state. The tuning curve of the neurons, as measured by averaging their activity between $t = 200\,\mathrm{msec}$ and $t = 400\,\mathrm{msec}$, is displayed in figure 13.21B; the width of this tuning curve is 50°. This response is the result of spontaneous symmetry breaking the translation invariance, as analyzed theoretically in "Homogeneous Input, Marginal Phase" (section 13.4.4). Note that the location of the activity profile displays random fluctuations. This is expected, since in the absence of a tuned stimulus, the noise in the network causes a slow random wandering of the profile along the marginal direction. Because this motion is a result of a coordinated change in the neuronal states, the time scale associated with it is proportional to $1/N$, where N is the number of neurons in the network.

Figure 13.22A shows the tuning curves of the neurons for different values of the tuning parameter ε. By comparing figures 13.21A and 13.22A, it can be seen that the system of figure 13.21A acts as if there were an external stimulus at a 30° orientation. The tuning width of the two figures is the same, indicating that it is determined by the cortical interactions. The weakly tuned stimulus fixes the position of the activity profile, selecting from among the set of attractors the one that best matches its own profile, namely, the one that peaks at the orientation column with the largest input. Figure 13.22A also shows that the width of the tuning curves of the neurons for different values of the tuning parameter ε remains almost the same, even for ε as large as 0.5. Indeed, in the presence of stimuli not too strongly tuned, it is almost independent of intensity even though the response of the neurons to stimuli at their preferred orientation can increase significantly when the intensity is increased (figure 13.22B). These properties of the tuning curve were predicted in the analytical solution of the rate model. Our simulations show that they remain valid in biophysically more realistic models that incorporate spikes.

Virtual Rotation In our simplified model, the system's transient response to a step change in stimulus orientation was an indicator of the mechanism of orientation selectivity. If the alignment of the afferent LGN input is the main mechanism, then following a change in the stimulus orientation, the activity in previously stimulated columns will decay, while the activity of the columns with PFs close to the new stimulus orientation will increase. If, on the other hand, the spatial modulation of

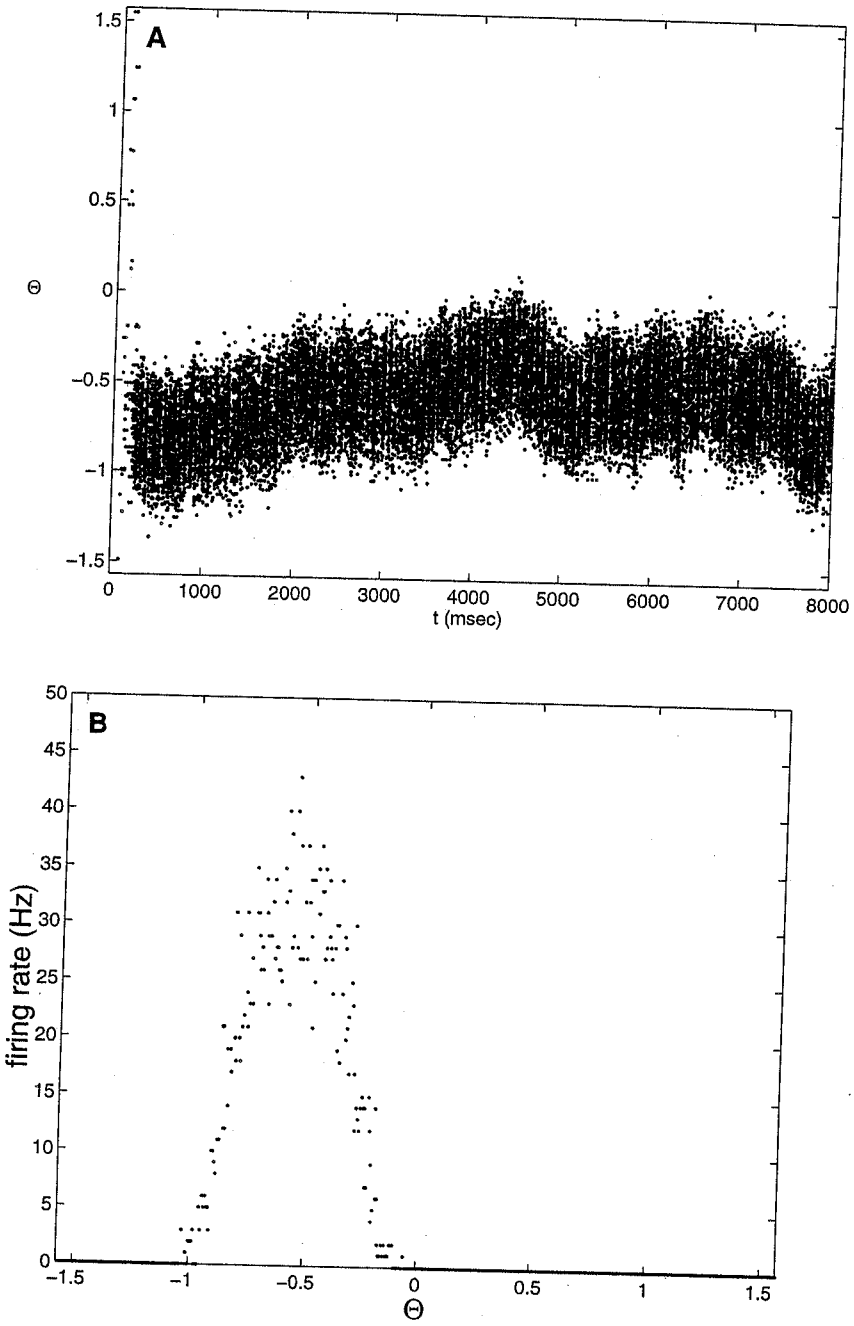

Figure 13.21
Response of the network to an homogeneous stimulus ($\varepsilon = 0$) in the marginal phase. Parameters are given in tables 13.1 and 13.2. Stimulus is presented at $t = 200$ msec. (A) Raster plot. (B) Activity profile averaged between $t = 200$ msec and $t = 400$ msec.

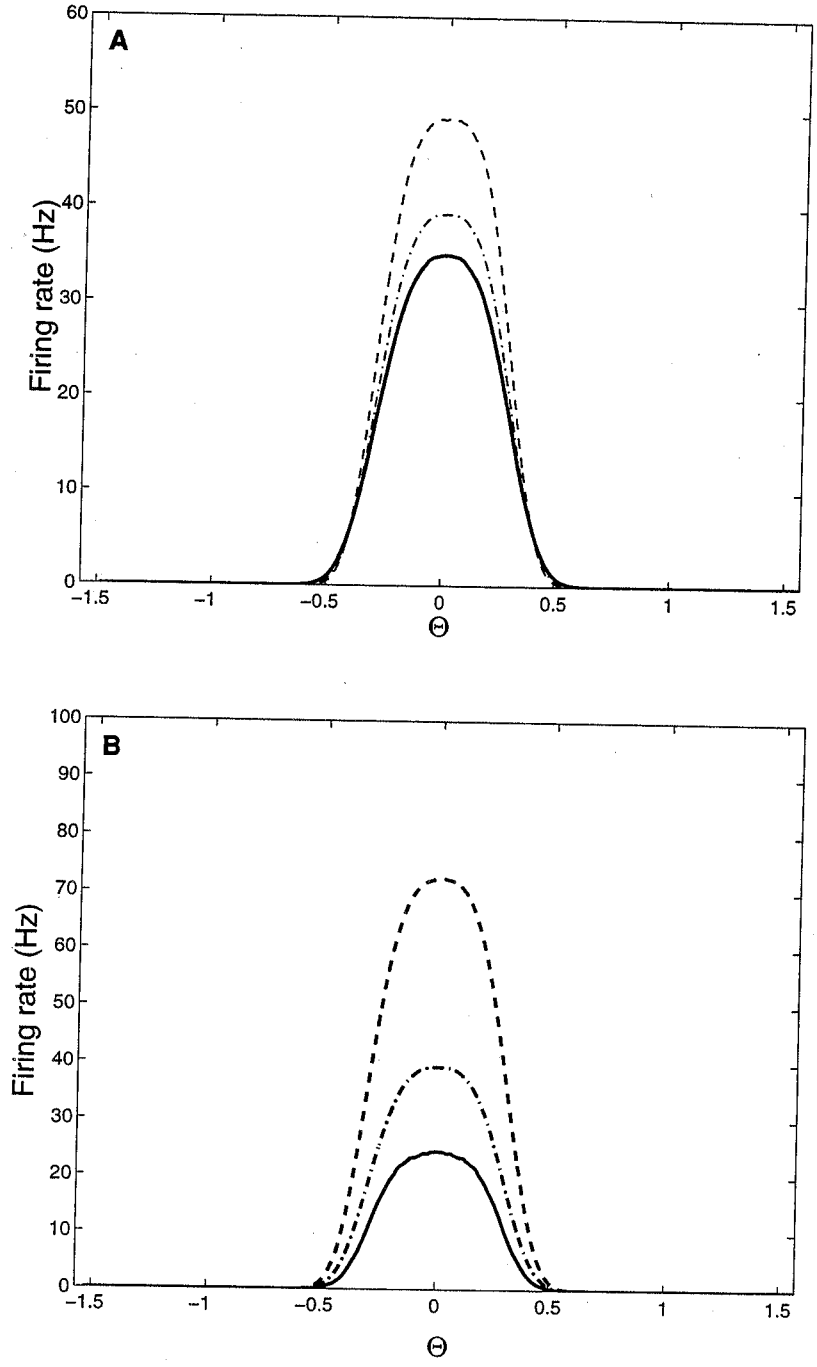

Figure 13.22
Marginal phase. Parameters are given in table 13.1 (chapter appendix C). (A) Tuning curve of a neuron ($\theta = 0^0$) for $\varepsilon = 0.05$ (solid line) $\varepsilon = 0.1$ (dash-dotted line) and $\varepsilon = 0.2$ (dashed line). The intensity is $C = 1{,}000$ Hz. (B) Tuning curve of a neuron ($\theta = 0^0$) for $C = 500$ Hz (solid line) $C = 1{,}000$ Hz (dash-dotted line) and $C = 2{,}000$ Hz (dashed line). The input tuning is $\varepsilon = 0.1$.

the cortical interactions plays a dominant role, then the population activity will move across the cortex, transiently activating the intermediate column until it settles in the new stable position.

To test whether this prediction also holds in our more realistic model, we have calculated the response of the system to changing of the stimulus feature. Figure 13.23A shows the evolution in time of the activity profile following a 60° change in the stimulus feature for a tuning parameter of the LGN input $\varepsilon = 0.1$, while figure 13.23B shows the evolution of the membrane potential for five neurons. Together, the figures clearly illustrate the phenomenon of virtual rotation. The velocity of the rotation depends on the input tuning, as we can see in figure 13.23C, where the trajectory of the maximum of the activity profile is plotted as a function of time, for different values of ε. To make a more quantitative comparison between these simulation results and our theory, we have computed the velocity V_C by fitting these trajectories according to eq. 13.69. We find that when ε is not too large, the angular velocity is inversely proportional to ε, which closely agrees with the theory of section 13.4.

13.7.5 Network with Adaptation-Intrinsic Moving Profiles

The theory of section 13.5.2 (see "Modeling Neuronal Adaptation") predicts that when single neurons display sufficiently strong or sufficiently fast firing adaptation, the response of the network to a weakly tuned input is a pulse of activity traveling across the network. Here we show that this result holds also in our more realistic network model of spiking neurons.

The raster plot of figure 13.24A corresponds to the network state when the stimulus is not tuned for typical adaptation parameters. It shows a pulse of activity of width $\theta_c = 30°$, which travels across the network at an angular velocity of $\omega = 9.2\,\text{rad/sec}$. For a given adaptation time constant, the velocity of the pulse decreases monotoncally with the adaptation maximal conductance (see figure 13.24B). For the corresponding set of parameters, the stationary state is destabilized for adaptation conductances as small as $g_a = 1.8\,\text{mS/cm}^2$, where the rate of adaptation is 5%, a value much smaller than what is observed in reality. For this value of g_a, $V_0 \approx 2.1\,\text{rad/sec}$. For small values of g_a, V_0 becomes small and hard to measure because of the noise in the network. The effect of this noise can be reduced only by increasing the network size. For instance, the result with the smallest g_a ($g_a = 1.8\,\text{mS/cm}^2$) in figure 13.24B was obtained in a network of $N_E = N_I = 2{,}048$ neurons by averaging the velocity of the pulse over 18 sec. Traveling pulses of activity exist for g_a as small as $1\,\text{mS/cm}^2$, but a quantitative evaluation of their velocity would have required even larger networks and longer time averaging.

Finally, we consider the effect input tuning has on these traveling pulses. For a sufficiently small value of ε, a pulse of activity can still propagate across the whole network. If we measure the tuning curve of neuron by averaging its response to stimuli with different features over different trials, we find it is extremely wide. For a sufficiently large value of ε, the traveling pulse is completely pinned around the column corresponding to the input feature (result not shown). This network state resembles what is obtained in the absence of adaptation. Finally, for intermediate values of ε, the profile of network activity performs oscillations around the angle corresponding to the stimulus feature (see figure 13.25). The tuning curve of the neurons, averaged over many trials, will show the right preferred feature but with a width greater than that of the network activity profile.

13.8 Discussion

We have studied how local excitatory and inhibitory feedback shapes the selective response of neurons to external stimuli. With regard to stationary states, we have found three qualitatively different regimes. In the first regime, the dominant feedback is afferent input; in the second, it is broad inhibition, which may, as a result, substantially sharpen the tuning of the neurons. Yet in both these regimes, the tuning width strongly depends on the *effective tuning* of the input, implying that decreasing the spatial modulation of the external input or increasing its overall intensity will broaden the tuning of the neuronal responses. As a corollary in both regimes, if the input is spatially homogeneous, the network activity will be uniform as well. The third, or marginal, regime is characterized by strong, spatially modulated excitatory feedback, leading to the emergence of an intrinsic line of stable states. Each of these states exhibits a single "hill" of activity whose width is determined by both the modulation amplitude and the spatial range of the cortical feedback, but whose height is linearly related to the stimulus intensity. Activating the network by a tuned input will select the profile whose peak coincides with that of the input. The width of the activity profile is substantially modified by the input only when the tuning provided by the afferent mechanism is significantly sharper than that of the intrinsic profile. Computationally, our work suggests a mechanism for generating a separable coding of several stimulus features (Salinas and Abbott 1996).

The intrinsic localized states in our models differ from those studied by Amari. In Amari's model (1977), the localized states appear exclusively as bistable where the stimulus is subthreshold and are characterized by a *saturated* activity of at least part of the network. In contrast, in our network, the stimulus is suprathreshold and all

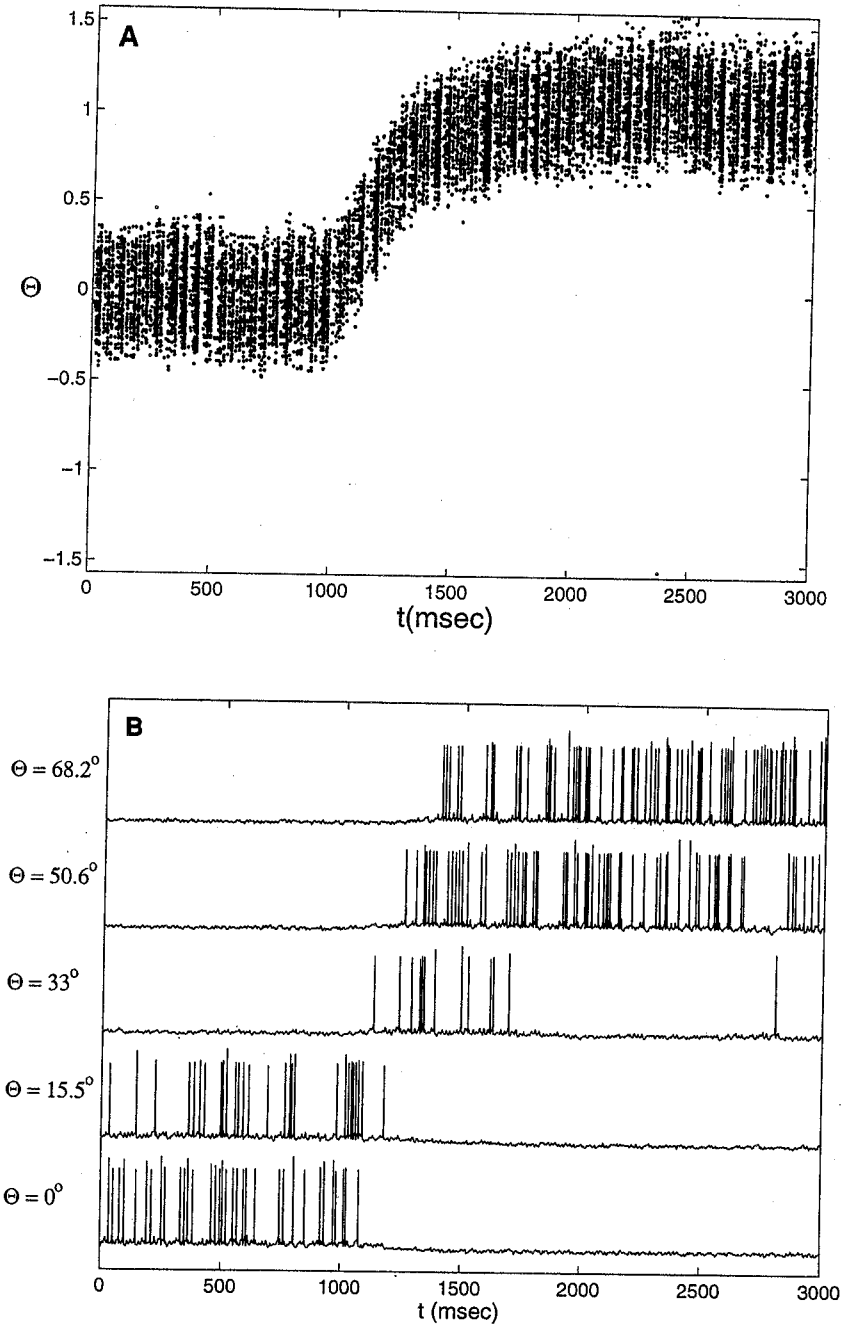

Figure 13.23
Virtual rotation in the marginal phase. Parameters are given in table 13.1 (chapter appendix C). The input intensity is $C = 1{,}000$ Hz. The stimulus is at $\theta_1 = 0^0$ and is suddenly turned to $\theta_2 = \pi/3$ at $t = 1$ sec. (A) Raster plot for $\varepsilon = 0.1$. (B) Trace of the membrane potentials of five neurons in the networks. (C) Trajectory of the population vector angle for $\varepsilon = 0.025$ and $\varepsilon = 0.2$.

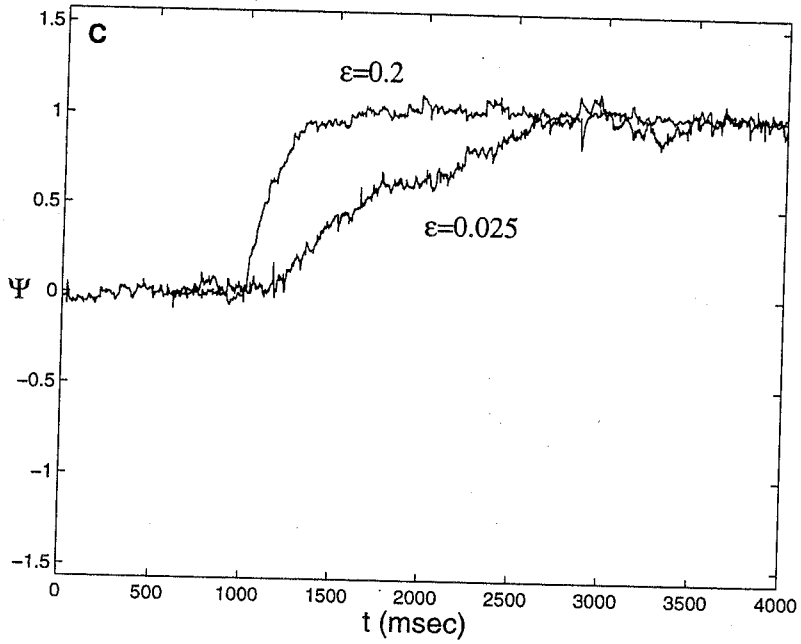

Figure 13.23 (continued)

the neurons are far below saturation, which leads to important differences in the properties of the localized states. In contrast to our network, in Amari's case, the width rather than the height of the activity profile depends strongly on the stimulus intensity. Another important difference is that in contrast to Amari's analysis, in our study stable states with multiple peaks do not exist. The reason for this is related to two features of our model: the above-mentioned unsaturated regime; and the long-range inhibition, which can stabilize a single hill of unsaturated neuronal activity, but not multiple hills.

The analytical work presented here used a one-population rate model, which contradicts the separation of excitation and inhibition in cortex. There are conditions, however, where the state of a two-population network can be exactly described by an equivalent one-population network. And even when these conditions are not met exactly, many qualitative properties of the stationary states may not differ, as is evident from our theoretical study of the full two-population model (Ben-Yishai, Hansel, and Sompolinsky 1997). The most important difference between these network types is that two populations may give rise to additional nonlinearities with respect to stimulus intensity. These effects may be functionally important. For instance, increasing stimulus intensity may suppress network activity. Also, in general, the invariance of the shape of the activity profile to changing the stimulus intensity

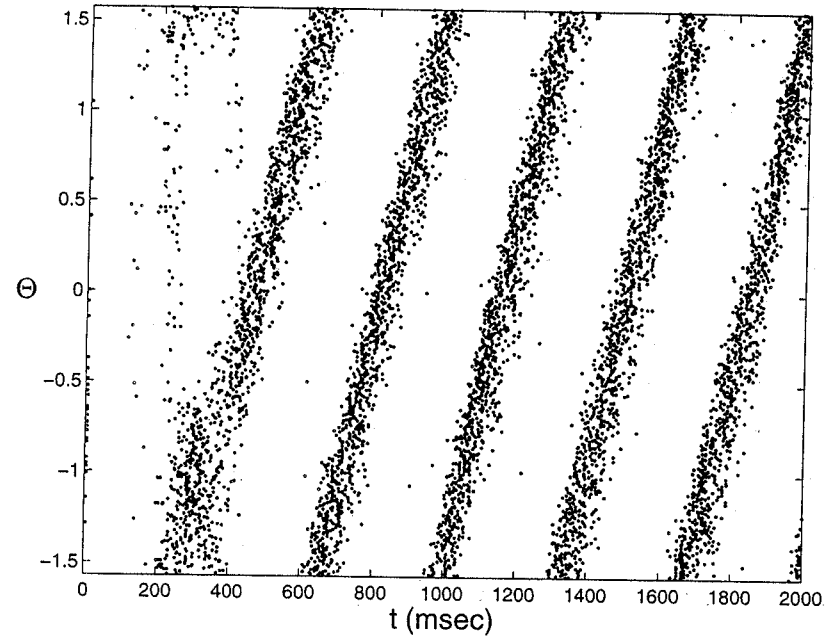

A

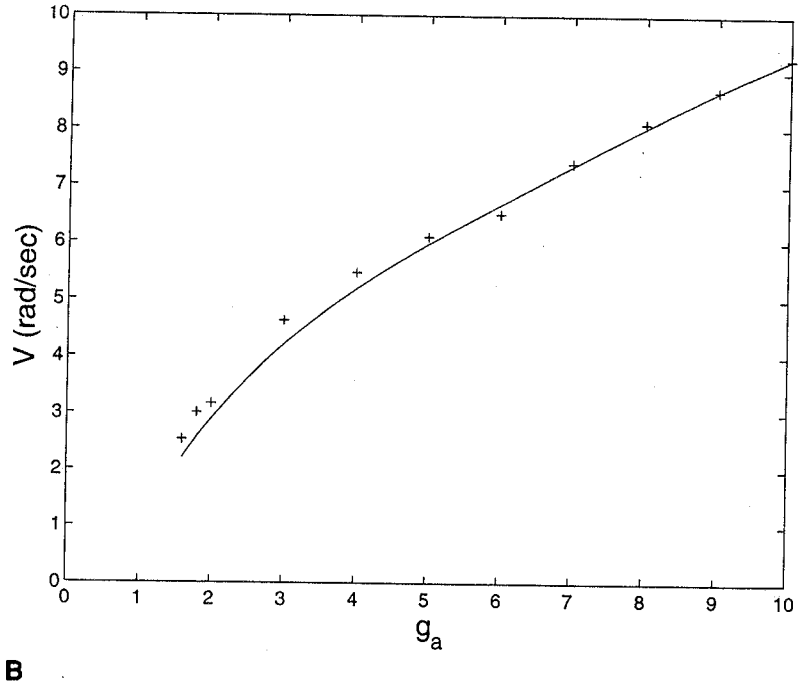

B

Figure 13.24
Traveling pulse of activity in the network model with spiking neurons. Parameters are given in table 13.1 (chapter appendix C). (A) Raster plot when the stimulus is homogeneous. Adaptation parameters: $g_a = 10\,\mathrm{mS/cm^2}$ and $\tau_a = 60\,\mathrm{msec}$. (B) Angular velocity of the wave as a function of the adaptation maximal conductance. Here $\tau_a = 60\,\mathrm{msec}$. The solid line is an interpolation of the simulation results.

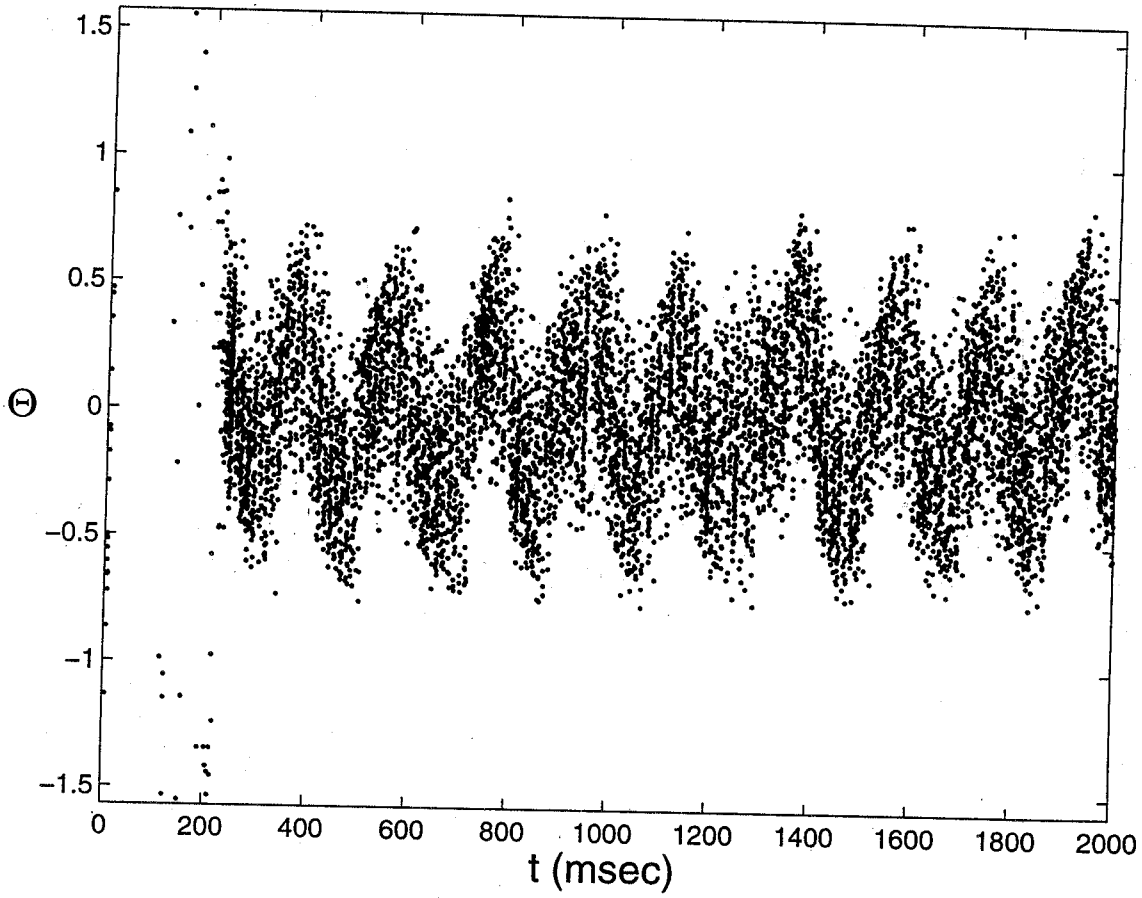

Figure 13.25
Pinning of the traveling pulse by inhomogeneous input. The parameters are as in figure 13.24A. The input tuning is $\varepsilon = 0.2$.

breaks down at low contrasts. Another important difference lies in the temporal domain. Whereas the symmetry of the connections of the one-population model (without adaptation) precludes the appearance of temporal attractors, the two-population model may give rise to spatiotemporal attractors such as the above-mentioned moving hills and various other oscillatory states. Here, too, the threshold nonlinearities of the inhibitory population lead to potentially important dependence of the moving hill's velocity on the stimulus intensity (see Ben-Yishai, Hansel, and Sompolinsky 1997 for more details).

We have show that a substantial spike adaptation may give rise to intrinsic traveling waves in the form of activity pulses that move with constant velocity. In fact, neuronal adaptation can be viewed as a form of local inhibitory feedback (present in addition to explicit global inhibition). In this model, as in the two-population model

mentioned above, the spatial dependence of the connections is symmetric. Therefore, the direction of propagation is determined by symmetry breaking, for example, by the initial conditions. An alternative mechanism for the generation of moving hills is provided by spatially asymmetric connections. If the pattern of connection is such that each neuron excites neighbors on its right more strongly than those on its left, the system may generate a traveling waves that always moves to the right. (Lukashin et al. 1996; Zhang 1996; Tsodyks et al. 1996)

Another simplification of our model is the description of the neuronal nonlinearity as a threshold linear gain function. This greatly simplifies the analytical study; the resultant dynamical equations are all linear except for one parameter, namely, the tuning width, whose value is given by an implicit nonlinear equation. This gain function is not a bad approximation of the rate-current characteristics of many cortical cells (Connors, Gutnick, and Prince 1982; Ahmed, Anderson, et al. 1994). Adding moderate nonlinearity to the neuronal suprathreshold gain function does not substantially change its behavior.

We have also analyzed the behavior of network models with conductance-based dynamics appropriate for cortical neurons. These models are too complex for a analytical study, we have nevertheless shown that under certain conditions these networks can in principle be described by a set of mean field self-consistent rate equations similar in spirit to those of the rate models. The qualitative similarity between simplified and realistic models is evident from the numerical simulation results. We have shown that the main qualitative predictions of the simplified rate models are manifest also in the realistic models, a conclusion also supported by the numerical simulations of Somers, Nelson, and Sur (1995), who have studied the role of cortical excitatory feedback in orientation selectivity in primary visual cortex using integrate-and-fire network models, with a more realistic modeling of the external input to the network. Earlier numerical investigations studied the role of cortical inhibition on orientation selectivity using integrate-and-fire network models (Wehmeier et al. 1989; Wörgötter and Koch 1991). One-dimensional networks of conductance-based neurons coding for the direction of movement have been simulated by Lukashin and Georgopoulos (1994). It should be emphasized, however, that all these models make similar simplifying assumptions about the local connectivity pattern in cortex; none incorporates potentially important synaptic dynamical properties such as short-term depression and facilitation.

We have limited our discussion to either stationary or coherent temporal behavior. In other studies (Ginzburg and Sompolinsky 1994; Ben-Yishai, Lev Bar-Or, and Sompolinsky 1995), it has been shown that the theory makes important predictions also with regard to the spatiotemporal spectrum of fluctuations in neuronal activ-

ities that can be tested by correlation measurements. Our numerical simulations have shown that these aspects can also be observed in the realistic networks (Hansel and Sompolinsky 1996). Thus the main spatiotemporal cooperative properties of these networks are the result of the architecture of connections rather than the details of the dynamics.

Line attractor neural networks have been also proposed as models of neural integrator circuits in the brainstem structures that control eye position (Robinson 1989; Seung 1996), where each state along the line represents one possible stable eye position. In the integrator models, it is proposed that the line attractor lies in a linearly marginally stable direction of the connection matrix. This mechanism relies on the system's being only weakly nonlinear. By contrast, the mechanism in our networks invokes the translational symmetry of the connections and is also present in strongly nonlinear regimes. Our study of the short-range model with open boundary conditions illustrates that the results are robust against boundary effects that break the symmetry. Nevertheless, it should be stressed that the existence of line attractor in both kinds of networks requires fine-tuning of some network parameters. In our networks, the existence of marginal phase is sensitive to local perturbations, such as nonuniform distribution of the representation of the preferred features (Zhang 1996; Lee et al. 1996; Tsodyks and Sejnowski 1995). Provided these perturbations are weak, however, the response of the system to an external stimulus may only be weakly affected, as long as the tuning bias generated provided by the stimulus is strong compared with those generated by the internal "imperfections." Ultimately, if line attractors are used for substantial computation, it is likely that their stability is maintained by an appropriate learning mechanism. Thus, even in sensory areas, the processing of stimuli may be intimately related to the short-term and long-term dynamics of the connections, an important topic outside the scope of this study.

Acknowledgments

This work is supported in part by the Fund for Basic Research of the Israeli Academy of Science and by the Centre National de la Recherche Scientifique: PICS "Dynamique neuronale et codage de l'information: Aspects physiques et biologiques." Most of the numerical simulations of section 13.7 have been performed on the supercomputers at the Institut de Développement et des Ressources en Informatique Scientifique; Orsay, France.

Many aspects of the work are based on research performed in collaboration with Rani Ben Yishai (see Ben-Yishai 1997) and Ruti Lev Bar-or (see Lev Bar-or 1993).

We have greatly benefited from many discussions with R. Ben Yishai, Sebastian H. Seung, and Carl van Vreeswijk. We acknowledge the hospitality of the Marine Biological Laboratory (Woods Hole, Mass.) during the summers of 1994, 1995, and 1996, where parts of this research were conducted. David Hansel acknowledges the very warm hospitality of the Racah Institute of Physics and the Center for Neural Computation of the Hebrew University.

Appendix A: Solution of the One-Population Rate Model

This appendix presents the details of the solution of the one-population model defined by eqs. 13.11–13.17.

General Time-Dependent Equations

We first consider the general case of stimulus with a time-varying feature $\theta_0(t)$. We write eq. 13.11 as

$$\tau_0 \frac{d}{dt} m(\theta, t) = -m(\theta, t) + [I_0(t) + I_2(t)\cos(2(\theta - \Phi(t)))]_+. \tag{13.A1}$$

By comparison with eq. 13.15, we obtain

$$I_0 = C(1 - \varepsilon) + J_0 r_0 - T \tag{13.A2}$$

$$I_2 = \varepsilon C \cos(2(\theta_0 - \Phi)) + J_2 r_2 \cos(2(\Psi - \Phi)), \tag{13.A3}$$

where, for simplicity, we have suppressed the time arguments. Note that, in general, r_0, θ_0, Ψ, and Φ are time-dependent. Phase Φ, the location at which the total input $I(\theta, t)$ (eq. 13.12) is maximum, is determined by the condition

$$0 = \varepsilon C \sin(2(\theta_0 - \Phi)) + J_2 r_2 \sin(2(\Psi - \Phi)). \tag{13.A4}$$

The case of broad-tuning where the input is above threshold for all θ and t is straightforward and will not be dealt with here. We focus on the case of narrow-tuning for which, by definition, there exists a value θ_C such that

$$I(\Phi \pm \theta_C, t) = I_0 + I_2 \cos(2\theta_C) = 0. \tag{13.A5}$$

Therefore, θ_C is given by

$$\theta_C = \frac{1}{2}\arccos(-I_0/I_2), \tag{13.A6}$$

and eq. 13.A1 can be written

$$\tau_0 \frac{d}{dt} m(\theta, t) = -m(\theta, t) + I_2(t)[\cos(2(\theta - \Phi(t))) - \cos(2(\theta_C(t))]_+. \tag{13.A7}$$

Dynamical equations for the order parameters (eq. 13.16) are derived by Fourier-transforming eq. 13.A7, which yields

$$\tau_0 \frac{dr_0}{dt} = -r_0 + I_2 f_0(\theta_C) \tag{13.A8}$$

$$\tau_0 \frac{dr_2}{dt} = -r_2 + I_2 f_2(\theta_C)\cos(2(\Phi - \Psi)) \tag{13.A9}$$

$$2r_2\tau_0 \frac{d\Psi}{dt} = I_2 f_2(\theta_C)\sin(2(\Phi - \Psi)), \tag{13.A10}$$

where

$$f_0(\theta c) = \int_{-\pi/2}^{+\pi/2} \frac{d\theta}{\pi}[\cos(2\theta) - \cos(2\theta_C)]_+ \tag{13.A11}$$

$$f_2(\theta_c) = \int_{-\pi/2}^{+\pi/2} \frac{d\theta}{\pi}\cos(2\theta)[\cos(2\theta) - \cos(2\theta_C)]_+. \tag{13.A12}$$

Performing the integrals, we find the the functions given in eqs. 13.39 and 13.40.

Stationary State

In the case of a stimulus with a constant feature θ_0, the solution of the above equations converges at large time to a fixed point, which is obtained by substituting the time derivatives in all the above equations by zero. From eqs. 13.A4 and 13.A10 we find

$$\Phi = \Psi = \theta_0. \tag{13.A13}$$

Another solution exists in which $\Phi = \Psi = \theta_0 + \pi$, but this solution is unstable, as can be seen from the next section. This means that in a stationary state the peaks of the profiles of both the total input and the output coincide with that of the stimulus. Thus eqs. 13.A2 and 13.A3 read

$$I_0 = C(1 - \varepsilon) + J_0 r_0 - T \tag{13.A14}$$

$$I_2 = \varepsilon C + J_2 r_2. \tag{13.A15}$$

Substituting this into eqs. 13.A8 and 13.A9 yields

$$r_0 = (C\varepsilon + J_2 r_2) f_0 \tag{13.A16}$$

$$r_2 = (C\varepsilon + J_2 r_2) f_2. \tag{13.A17}$$

$$\tag{13.A18}$$

For $\varepsilon > 0$, the solution is

$$r_2 = \frac{C\varepsilon f_2(\theta_C)}{1 - J_2 f_2(\theta_C)} \tag{13.A19}$$

$$r_0 = \frac{C\varepsilon f_0(\theta_C)}{1 - J_2 f_2(\theta_C)}. \tag{13.A20}$$

Replacing r_0 and r_2 by these expressions in eq. 13.A6, we obtain the equation for the width of the activity profile. The stationary profile has the form of eq. 13.36, and the gain G is

$$G = I_2(1 - \cos(2\theta_C)), \tag{13.A21}$$

yielding for the gain G the expression given in eq. 13.42.

For $\varepsilon = 0$, eq. 13.A17 always has a homogeneous solution, $r_2 = 0$, because the system is invariant by rotation. From eq. 13.A19, however, we see that an inhomogeneous solution ($r_2 \neq 0$) can also exist, provided that

$$1 = J_2 f_2(\theta_C). \tag{13.A22}$$

Eq. 13.A22, which corresponds to eq. 13.55, determines θ_C in the marginal phase and possesses a solution only if $J_2 > 2$. In this regime, r_0 and r_2 are determined by eq. 13.A6, 13.A14, and 13.A15, with $\varepsilon = 0$ and

$$r_0 = J_2 r_2 f_0. \tag{13.A23}$$

Substituting the results in eq. 13.A21 yields, finally, eq. 13.56.

Response to Moving Stimulus

We consider here the solution of the time-dependent eqs. 13.A8–13.A10 in the case of time-dependent stimulus feature $\theta_0(t)$. Eqs. 13.A10 and 13.A4 yield

$$\tau_0 \frac{d\psi(t)}{dt} = -V_C \sin(2(\theta_0(t) - \Phi(t))), \tag{13.A24}$$

where

$$\tau_0 V_C = \frac{\varepsilon C I_2 f_2(\theta_C)}{2 J_2 r_2^2}. \tag{13.A25}$$

Although, in general, V_C is itself a function of time, when $|\tau_0 \, d\theta_0/dt| = O(\Upsilon) \ll 1$, the time dependence of V_C introduces corrections of order Υ to V_C. To leading order, V_C is given by substituting the value of r_2 at order Υ, which in turn is given according to eq. 13.A9 (with $\Phi = \Psi$ and $dr_2/dt = 0$) by $r_2 = I_2 f_2$. Substituting this value yields $\tau_0 V_C = \varepsilon C / 2 J_2 r_2$. Finally, using eqs. 13.55–13.57, we obtain eq. 13.65.

Appendix B: Stability of the Stationary States

This appendix presents the stability analysis for the stationary states of the one-population rate model with neuronal adaptation given by eqs. 13.75–13.76 and 13.12–13.14.

Stability of the Broad Profile

When the system has a broad profile, all the neurons are above threshold and the system operates in the linear regime. Thus small perturbations around the linear fixed point of eqs. 13.75 and 13.76 obey the linear equations

$$\tau_0 \frac{d}{dt} \delta m(\theta, t) = -\delta m(\theta, t) + J_0 \delta r_0 + J_2 \delta r_2 \cos(2\theta) + J_2 r_2 \sin(2\theta) \delta\Psi - \delta I_a(\theta, t) \tag{13.B1}$$

$$\tau_a \frac{d}{dt} \delta I_a(\theta, t) = -\delta I_a(\theta, t) + J_a \delta m(\theta, t). \tag{13.B2}$$

The solutions of these equations can be written in the form

$$\delta m(\theta, t) \propto e^{\gamma t} \tag{13.B3}$$

$$\delta I_a(\theta, t) \propto e^{\gamma t}. \tag{13.B4}$$

The homogeneous fixed point is stable if and only if $Re\,\gamma < 0$. Solving eq. 13.B2 for δI_a and substituting in eq. 13.B1 yields

$$(1 + \Gamma(\gamma)) \delta m(\theta, t) = J_0 \delta r_0 + J_2 \cos(2\theta) \delta r_2 + J_2 r_2 \sin(2\theta) \delta\Psi, \tag{13.B5}$$

where

$$\Gamma(\gamma) \equiv \gamma\tau_0 + \frac{J_a}{1+\gamma\tau_a}. \tag{13.B6}$$

Fourier-transforming this equation gives

$$(1+\Gamma(\gamma))\delta r_0 = J_0\delta r_0 \tag{13.B7}$$

$$(1+\Gamma(\gamma))\delta r_2 = \frac{J_2}{2}\delta r_2 \tag{13.B8}$$

$$(1+\Gamma(\gamma))\delta\Psi = \frac{J_2}{2}\delta\Psi. \tag{13.B9}$$

(Eq. 13.B9 has to be considered only if $\varepsilon \neq 0$.) Thus the two Fourier modes of fluctuations are decoupled and the condition that δ_2 relaxes is identical to the condition for $\delta\Psi$ to relax.

The first mode corresponds to a homogeneous fluctuation of the neuron activity. Here γ is the solution of

$$1+\Gamma(\gamma) = J_0. \tag{13.B10}$$

Therefore, in this mode, γ is determined by a second-order algebraic equation. Solving this equation, we see that, depending on the strength of the adaptation, the broad state may lose stability in two ways.

Case 1. $J_a < \tau_0/\tau_a$: γ is real and is negative only for $J_0 < 1 + J_a$. In particular, when there is no adaptation, we recover the result of eq. 13.34.

Case 2. $J_a > \tau_0/\tau_a$: γ is complex on the instability line which is given by

$$J_0 = 1 + \frac{\tau_0}{\tau_a}. \tag{13.B11}$$

On this instability line, the system enters into a global oscillatory state.

The second mode of instability corresponds to a spatial instability. For this mode, γ is determined by

$$1+\Gamma(\gamma) = \frac{J_2}{2}. \tag{13.B12}$$

Here also, two cases have to be distinguished:

Case 1. $J_a < \tau_0/\tau_a$: γ is real on the instability line given by

$$J_2 = 2(1+J_a). \tag{13.B13}$$

This instability corresponds to the fact that if $J_2 > 2(1+J_a)$, the system prefers a narrowly tuned stationary state over the broadly tuned one, even when the input is homogeneous. In particular, for $J_a = 0$, we find eq. 13.35.

Case 2. $J_a > \tau_0/\tau_a$: γ is complex on the instability line given by

$$J_2 = 1 + \frac{\tau_0}{\tau_a}. \tag{13.B14}$$

This line is drawn in figure 13.11. For J_2 larger than this value, the system prefers a narrowly tuned state which, because γ is complex, is nonstationary and consists of a traveling pulse of activity. On the instability line, the velocity of the pulse is given by the imaginary part of γ, yielding eq. 13.83.

Stability of the Marginal Phase

We discuss here the stability of the narrow profile in the marginal phase. We first discuss the case of $\varepsilon = 0$ and $J_a = 0$. We linearize eqs. 13.A8–13.A10 about the fixed point of the marginal phase, eqs. 13.36 and 13.41 with eqs. 13.54–13.57, and we find

$$\tau_0 \frac{d\delta r_0}{dt} = -\left(1 - \frac{2J_0\theta_c}{\pi}\right)\delta r_0 + \frac{J_2}{\pi}\sin(2\theta_c)\delta r_2 \tag{13.B15}$$

$$\tau_0 \frac{d\delta r_2}{dt} = \frac{J_0}{\pi}\sin(2\theta_c)\delta r_0 - \left(1 - \frac{J_2}{\pi}\left(\theta_c + \frac{1}{4}\sin(4\theta_c)\right)\right)\delta r_2 \tag{13.B16}$$

$$\tau_0 \frac{d\delta\Psi}{dt} = -(1 - J_2 f_2(\theta_c))\delta\Psi = 0. \tag{13.B17}$$

In eq. 13.B17 we have used the relationship between θ_c and J_2 (eq. 13.55). This equation implies that the fluctuations keeping the shape of the activity profile but changing the position of its peak (also called "transverse fluctuations") are marginal, that is, they do not decay with time. The "longitudinal fluctuations," representing perturbations of the shape of the profile, evolve according to eqs. 13.B15–13.B16. Searching for a solution of the form $\delta r_0, \delta r_2 \propto e^{\gamma t}$, we find that γ satisfies the second-order algebraic equation

$$\gamma^2 + \left(3 - \frac{\theta_c}{\pi}(J_0 + J_2)\right)\gamma + \frac{J_2}{\pi}\sin(2\theta_c) f_0(\theta_c)(J_C - J_0) = 0, \tag{13.B18}$$

where J_C is given by eq. 13.57. Solving eq. 13.B18, we find that the instability occurs when γ is real and becomes positive, that is, on the line

$$J_C = J_0. \tag{13.B19}$$

This line is drawn in figure 13.7: it separates the marginal phase from the amplitude instability region.

The above stability analysis can be straightforwardly extended to include the case of inhomogeneous input. In particular, the transverse fluctuations still decouple from the longitudinal fluctuations; they evolve according to

$$\frac{d\delta\Psi}{dt} = -\frac{\delta\Psi}{\tau_\Psi}, \tag{13.B20}$$

where

$$\tau_\Psi = \frac{\tau_0}{\Upsilon}\frac{G}{(1 - \cos(2\theta_c))} > 0. \tag{13.B21}$$

Thus the external tuned input stabilizes the transverse fluctuations, whose relaxation time τ_Ψ is proportional to $1/\Upsilon$ and diverges as $\Upsilon \to 0$, in agreement with eq. 13.B17.

Instability of the Marginal Phase Due to Adaptation

We now extend the previous analysis to include adaptation. We will show that if $\varepsilon = 0$, the transverse fluctuation mode of the inhomogenous fixed point is unstable if

$$J_a > \frac{\tau_0}{\tau_a}. \tag{13.B22}$$

This condition corresponds to the vertical line drawn on figure 13.11. As will be shown, this result is general and independent of the form of interaction and the boundary conditions.

A narrow profile has the form

$$m(\theta) = \frac{I_a(\theta)}{J_a} = M(\theta - \Psi), \tag{13.B23}$$

where $M(\theta)$ satisfies

$$M(\theta) = \frac{1}{1 + J_a} \int_{-\theta_c}^{\theta_c} J(\theta - \theta') M(\theta')\, d\theta'. \tag{13.B24}$$

If we differentiate eq. 13.B24 with respect to θ and integrating by part the right-hand side, using $M(\theta_c) = M(-\theta_c) = 0$, we find

$$M'(\theta) = \frac{1}{1 + J_a} \int_{-\theta_c}^{\theta_c} J(\theta - \theta') M'(\theta')\, d\theta'. \tag{13.B25}$$

The fluctuations which maintain the shape of the profile but change its position have the form

$$\delta m(\theta, t) = M'(\theta - \Psi)\delta\Psi(t) \tag{13.B26}$$

$$\delta I_a(\theta, t) = J_a M'(\theta - \Psi)\delta\Psi_a(t) \tag{13.B27}$$

If we linearize the dynamical equations, using eq. 13.B25 and the fact that $M'(\theta) \neq 0$, we find that

$$\tau_0 \frac{d\delta\Psi}{dt} = J_a \delta\Psi - J_a \delta\Psi_a \tag{13.B28}$$

$$\tau_a \frac{d\Psi_a}{dt} = -\delta\Psi_a + \delta\Psi. \tag{13.B29}$$

These equations imply that the longitudinal mode is unstable if the condition given by eq. 13.B22 is satisfied. Note that this proof holds for any form of interaction and that it is also independent of the boundary conditions, hence it applies also to the short-range model of section 13.6. However, it crucially relies on the gain functions being semilinear.

Appendix C: Details of Conductance-Based Model

This appendix presents the details of the model, given by eqs. 13.1–13.4, we have used in our numerical simulations. The voltage-gated current in eq. 13.110 is of the form

$$I^{\alpha}_{gated}(\theta, t) = \sum_{l=1}^{n} G^{\alpha}_{l}(V^{\alpha}(\theta, t))(V^{\alpha}(\theta, t) - V^{\alpha}_{l}), \tag{13.C1}$$

where G_l and V_l are the voltage-gated conductances and the reversal potentials of the various ionic currents that contribute to I_{gated}, detailed below (see also table 13.1).

Sodium Current: $I_{Na} = g_{Na} m^3 h (V - V_{Na})$

The inactivation variable h follows the first-order relaxation equation

$$\frac{dh}{dt} = \Delta \frac{h_\infty(V) - h}{\tau_h(V)} \tag{13.C2}$$

$$h_\infty(V) = \frac{a_h(V)}{a_h(V) + b_h(V)} \tag{13.C3}$$

Table 13.1
Parameter and constant values for conductance-based cortical network model

	E	I	m	
g_{N_a}	120	120	τ_1^e	3
g_K	10	20	τ_2^e	1
g_A	60	40	τ_1^i	7
g_{N_aP}	0.5	0.2	τ_2^i	1
g_l	0.1	0.1	g_{EE}	2
g_z	10	0	g_{EI}	1.3
V_{N_a}	55	55	g_{II}	0.8
V_K	−70	−70	g_{IE}	1
V_A	−75	−75	V_{syn}^e	0
V_l	−65	−65	V_{syn}^i	−75

$$\tau_h(V) = \frac{1}{a_h(V) + b_h(V)} \tag{13.C4}$$

$$a_h = 0.07\, e^{(-(V+55)/20)} \tag{13.C5}$$

$$b_h = 1/(1 + e^{(-(V+25)/10)}). \tag{13.C6}$$

To simplify the dynamics, we assume that the activation variable m is fast and equal to its instantaneous equilibrium value, given by

$$m_\infty(V) = \frac{a_m(V)}{a_m(V) + b_m(V)} \tag{13.C7}$$

$$a_m(V) = 0.1\, \frac{(V+30)}{1 - e^{(-(V+30)/10)}} \tag{13.C8}$$

$$b_m(V) = 4e^{(-(V+55)/18)}. \tag{13.C9}$$

The factor Δ has been introduced in order to tune the maximum firing rate to the desired high value. We use $\Delta = 4$.

Delayed-Rectifier Potassium Current: $I_K = g_K n^4 (V - V_K)$

The inactivation variable n satisfies

$$\frac{dn}{dt} = \Delta\, \frac{n_\infty(V) - n}{\tau_n(V)} \tag{13.C10}$$

$$n_\infty(V) = \frac{a_n(V)}{a_n(V) + b_n(V)} \tag{13.C11}$$

$$\tau_n(V) = \frac{1}{a_n(V) + b_n(V)} \tag{13.C12}$$

$$a_n = 0.01 \frac{(v+45)}{1 - e^{(-(V+45)/10)}} \tag{13.C13}$$

$$b_n = 0.125 e^{(-(V+55)/80)}. \tag{13.C14}$$

A-Current: $I_A = g_A ab(V - V_A)$

We assume activation is instantaneous and satisfies

$$a = a_\infty(V) = \frac{1}{1 + e^{(-(V+50)/4)}}. \tag{13.C15}$$

We further assume the relaxation time of the inactivation variable is independent of the membrane potential: $\tau_b = 10$ msec, and satisfies

$$\frac{db}{dt} = \frac{b_\infty(V) - b}{\tau_b} \tag{13.C16}$$

$$b_\infty = \frac{1}{1 + e^{((V+70)/2)}}. \tag{13.C17}$$

Persistent Sodium Current: $I_{NaP} = g_{NaP} s_\infty(V)(V - V_{Na})$

The activation variables satisfies

$$s_\infty(V) = \frac{1}{1 + e^{(-0.3(V+50))}}. \tag{13.C18}$$

Slow Potassium Current: $I_z = g_z z(V - V_K)$

This currents is incorporated into the dynamics of the excitatory population. The activation variable z satisfies the relaxation equation

$$\frac{dz}{dt} = \frac{z_\infty(V) - z}{\tau_z}, \tag{13.C19}$$

where $\tau_z = 60$ msec is independent of the membrane potential and

$$z_\infty(V) = \frac{1}{1 + e^{(-0.7(V+30))}} \tag{13.C20}$$

Note that the sodium current and the potassium delayed rectifier have the same parameters as in the Hodgkin-Huxley model, except for a shift of the membrane potential by 55 mV. This shift ensures that the threshold to spike is in the range observed in cortical neurons. Membrane potential is measured in millivolts.